TEKNOFEST

AEROSPACE AND TECHNOLOGY FESTIVAL

HELICOPTER DESIGN COMPETITION

FINAL DESIGN REPORT

TEAM NAME: HELLY-800

TEAM ID: T3-28250-193

TEAM MEMBERS:

1. **SONGÜL USLU**
2. **EZGİ HANDAN SAVAŞ**
3. **BASHIR ABDI ALI**
4. **MUHAMMAD TALHA AHMED ANSARI**

ADVISOR NAME:

Asst. Prof. Dr. ANNA PRACH
Aerospace Engineering Department Coordinator

TEAM LEADER NAME SURNAME:

SONGÜL USLU

TABLE OF CONTENTS

1. DESIGN DESCRIPTION

This final report is prepared for the "Teknofest Helicopter Competition 2020" by the HELLY-800 design team to design a high-performance helicopter for express cargo delivery and just-in-time logistics. The design requirements include minimum 3 hours endurance, 800 km range, and 400 km/h speed. A tilt-rotor helicopter concept is chosen due to its superior performance characteristics such as range, cruise speed, and endurance. A tilt- rotor helicopter combines the advantages for both turboprop aircraft and helicopter. This configuration incorporates hovering, vertical takeoff and landing capabilities, as well as allows to achieve high speed forward flight. The main features of the design include:

- **Higher Forward Speed**: The minimum forward speed requirement is 400 km/h. For conventional helicopters, this value is considered as the upper forward speed limit due to the aerodynamic limitations as a result of the induced shock wave flow separation on the advancing side, retreating blade stall, and reverse flow region on the retreating side. For a tiltrotor concept, the rotors are tilted forward and operate as the propellers of a conventional turboprop airplane in cruise flight.
- **More Range**: The improved cruise efficiency is achieved using two highly efficient turbo shaft engines. The new generation engine PW210A is selected for the design.

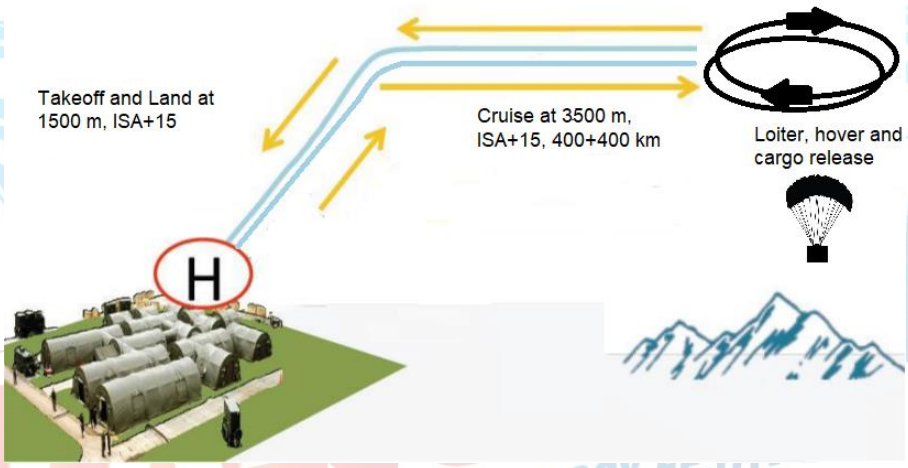

Figure 1 : Mission profile

- **Higher Fuel Efficiency**: is achieved by minimizing the overall weight, and selecting the engines with low specific fuel consumption.
- **One-engine Inoperative Flight**: the engines are connected with a shaft from one engine's gearbox to the other, therefore, in an event of failure of one engine, the second engine is able to drive both rotors.
- **Autorotation Capability**: The main rotors' blade pitch control mechanism and rotor drive systems must allow fast entry into autorotation in an event of power failure.
- **Noise Reduction**: Tiltrotors are inherently less noisy than conventional helicopters due to the absence of high frequency noise from the tail rotor. In addition, low vibrations level of the selected engine contributes to the noise reduction.
- **Emissions**: The selected engine PW210A is based on the green engine technologies, and has low fuel consumption and reduced environmental emissions.

- **Light Weight Material Selection**: **Material Selection:** The material selection of the helicopter depends on many specific design factors. For the selection, the criterias were mainly: fatigue resistance, strength, lightweight, stiffness manufacturability, and lower life cycle cost. HELLY-800 design compromises with all design considerations.

Material	Usage
Carbon/glass prepregs, Nomex honeycomb,Redux bonded assembly	Wings
Kevlar and Nomex honeycomb	Fuselage cabin floor
Carbon Prepregs, Al-Li alloys	Pressure Bulkhead, Stringers, Longeron
Fiber Glass	Vertical Stabilizer & Horizontal Stabilizer
Special process honeycomb and Redux bonded assembly.	Landing Gear Doors and Leg Fairings
Fibrelam panels	Cargo Flouring
Carbon Fiber	Rotor Blades
Rubber	Rotor hub bearings
M50-NiL	Transmission Gears
Hyper-elastic rubber	Landing Gear

- **Autorotation and engine failure:** This is the state of rotors operating when thee is no power produced by the engine. The power to produce the thrust and turn the rotor is supplied by descent of the helicopter during engine. Helly-800 design permits freewheeling unit that allows the main rotor to continue turning even if the engine is not running mechanically. There for the helicopter can safely be landed by the pilot in the event of egine failure. This is done in order to be certified.

2. SUBSYSTEMS

2.1.1 Landing gears

Helly-800 is designed with retractable landing wheels like aircrafts. Retractable landing wheels allows the design to maintain a low drag profile at high forward flight speeds. This landing wheels make helly-800 to be parked easily. The figure below shows the retractable landing wheels. This landing gear allow the helicopter to fly at much higher forward speeds for less power due to the reduction in parasite drag. They are relatively cheaper and reduce the weight of the helicopter as well as lowering the manufacturing costs.

Figure 2: Retractable landing wheels

The T-tail structure, as shown above, allows the design to have improved structural efficiency and reduced weight of the structure.

2.1.2 Power Transmission

Helly-800's transmission transfers power from the engines to the rotors. The two gearboxes, on the wing tips, step down the speed of the rotor so that it does not rotate same speed as the engine shaft. In addition, the RPM is reduced to prevent the tips of the blades from spinning faster than the speed of sound.

2.1.3 Rotor Configuration and Type

Helly-800 design uses combined rotor system with elastomeric bearings. The main rotor system uses combined principles of different rotor systems. It incorporates a flexible hub which allows for blade bending (flexing) without the need for bearing or hinges.

Elastomeric bearings are used to replace conventional roller bearings. They require no lubrication, therefore, require less maintenance. They also absorb vibration which means less fatigue and longer service life for the Helly-800 components.

Features and benefits:

- Reduced maintenance – it requires no lubrication
- Longer life – Its impervious to contaminants that would ruin traditional bearings
- Easy inspection - Visual inspection indicates approaching end of life
- Controllable dynamic properties - Stiffness and damping are engineered for the applications.

2.1.4 Dual hydraulic actuators

Double actuators are used, when transitions from helicopter mode to forward flight mode, to tilt the nacelle. The nacelle gearbox steps the RPM of the engine to the required RPM of the rotor in three stages.

Two planetary and split torque stage allowed Helly-800 design of an efficient, and light weight gearbox.in addition, the planetary ring, to reduce its weight and size, is incorporated with the gearbox casing.

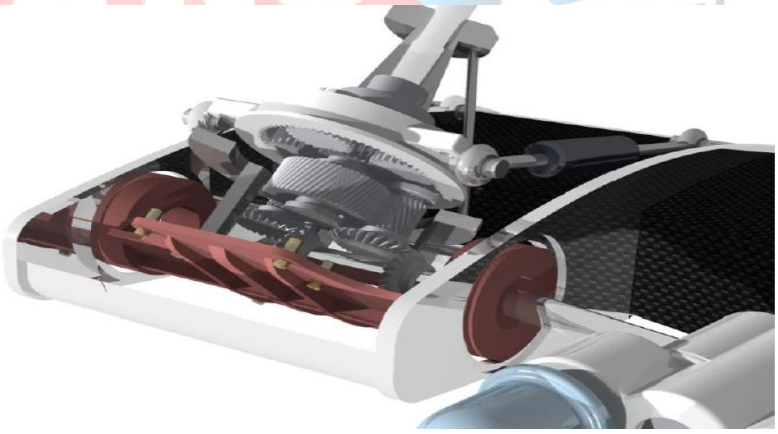

Figure 3: Dual hydraulic actuators [13]

2.1.5 Propulsion systems

Helly-800 is designed with turboshaft engine. This engine is a form of gas turbine which produces shaft power, that is used to drive the rotors, rather than jet thrust. This design is with increased reliability and minimum cost. Turboshart 2× PW 210 is selected since it produces 1000 Hp which is suitable for this

design. The extra power is transmitted to drive subsystems and for use in other flight condition. The two engines are placed on the tips of the wing span.

The turboshaft engine is similar to turbojet, with additional turbine expansion to extract energy from the exhaust and convert it into output shaft power. The following figure shows different sections of the turboshaft engine.

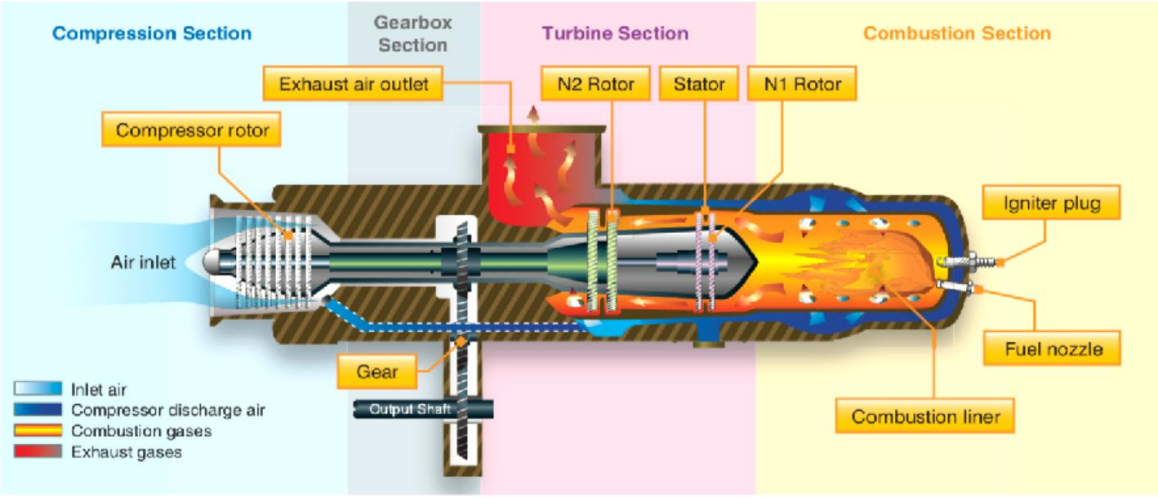

Figure 4: Different sections of turboshaft engine [3]

2.1.6 Ground clearance

For the design of Helly-800, the wings, fuselage and rotors are maintaned in such a way that there is enough distance between the landing surfaces and the rotors. The rotors will be in up position during landing and takeoff and remain in vertical position when the engine is off as shown in the figure below. In addtion, during droping of the carge there a clearance distance between the rotors and the cargo gate surfaces.

2.1.7 Control surfaces

Control surfaces, the aerodynamice devices, allow the pilot to control altitude, and direction of the helicopter. These control surfaces include flaps, slats, ailerons, rudders, stabilizers and elevators. The **figure 6** below shows all the control surface and their locations.

2.1.8 Cargo loarding and droping systems

The cargo loading is performed manually before each sortie on the ground before takeoff. The gates of the cargo bay are kept open. At this point where the locking mechanism of the cargo container that is attached to the parachute. The cargo is brought to the aircraft using means of transport as it is heavy to be directly carried. Once this Is complete. The cargo container is lifted to the position at which it is to be locked into the roof of the cargo bay. The lifting of the cargo is done using a mechanical jack. Once the cargo is in position it is locked and sealed with mating to the cargo bay. Once the cargo is fastened the doors of the cargo bay are closed and the aircraft is prepped for takeoff.

The cargo is to be delivered during cruise flight by performing a flyby. The cargo is equipped with a parachute which is opened once the cargo is released from the aircraft. Upon approach to the drop zone the pilot opens the cargo bay enough to provide clearance for cargo drop. With winds and other conditions in mind. The pilot releases the cargo using avionics and controls from the cockpit, so that it can land at the expected target site. Once the cargo is released after clearing the zone of the helicopter, the parachute is deployed and opens up (this is self-programmed). Upon release the pilot then proceeds to shut the gates of the cargo bay and proceeds with flight as per instructions.

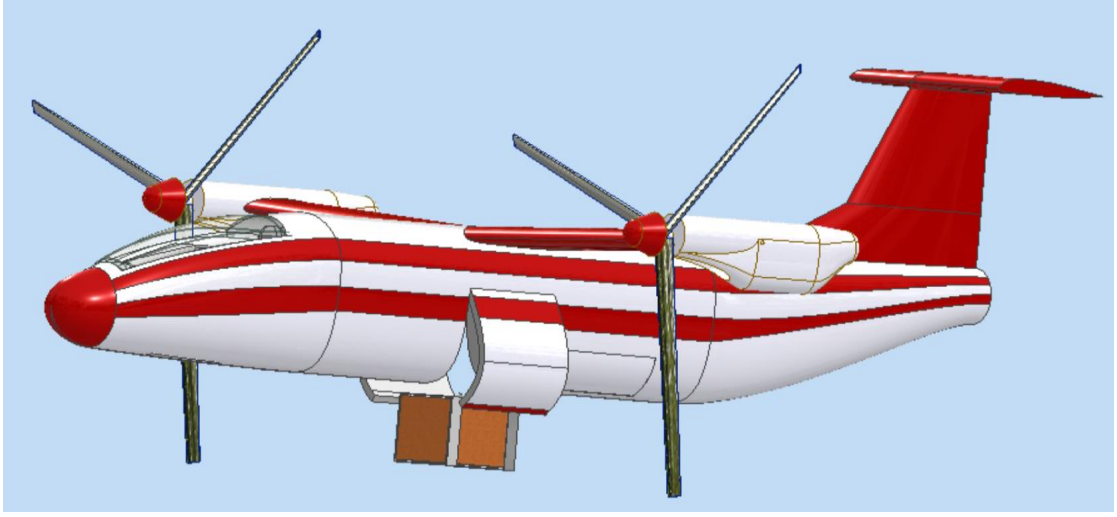

Figure : Cargo releasing mechanism

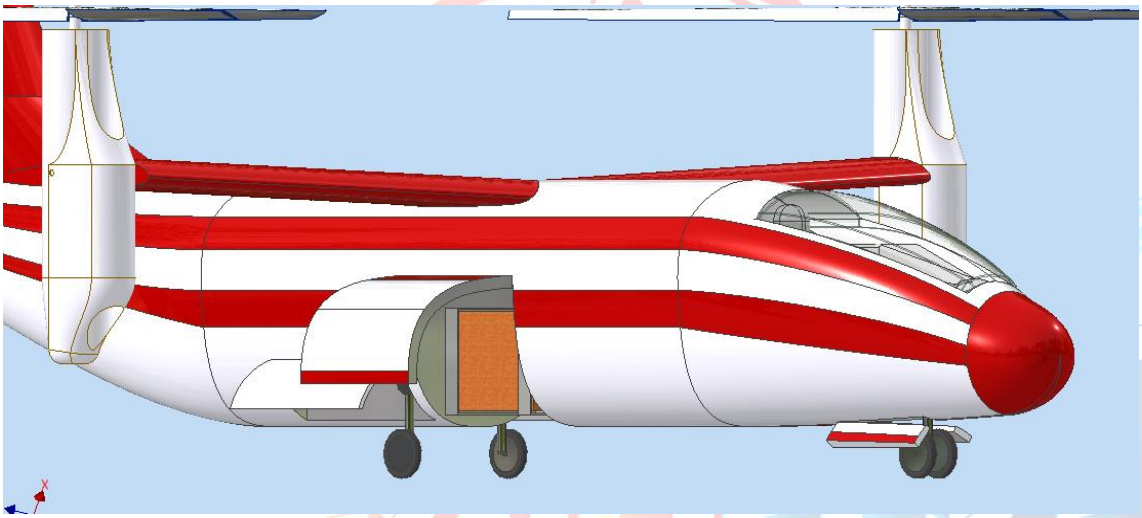

Figure : Cargo loading mechanism

2.1.9 Fuel tanks

The fuel that will be used for the flight mission will be stored in the fuel tanks on the wing. There are four tanks with volumes since their shapes are identical. The fuel used by the engine is taken from these tanks proportionally so that the cetre of gravity of the helicopter doesn't change. The figure below shows the fuel tanks.

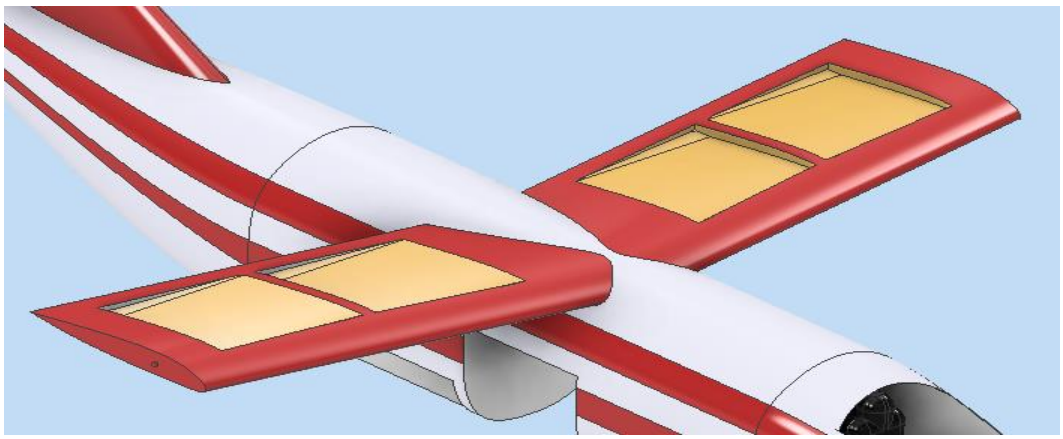

Figure : Fuel tanks

2.1.10 Maximizing the cargo volume

Cargo containers are placed close to the wings so that the position of the helicopter's center of gravity does not change. Helicopter sizing is optimized according to weight components, the required speed, and range requirements. Increasing the cargo container volume from 1.5 m^3 volume to 2 m^3 does not affect the fuselage size significantly. However, a cargo container larger than 2 m^3 causes the body volume to increase, unnecessarily increasing the total weight and consequently increase the drag coefficient, that is, the total drag. At the end of all these attempts, it is decided to maximize the cargo volume up to 2 m^3 to make human operation easier in cargo loading and to place cargos with different densities.

3. AVIONICS

Avionics and control system are essential parts in the design of any helicopter in order to perform its mission. Thus, a perfect selection of the avionics suite and control systems is a crucial requirement. When we do the selection process, we consider all necessary elements such as safety precaution, performance efficiency, purchasing and operational costs. There is a technologic development in this sector and a lot of designs are made to meet the customer needs. Below we will discuss our choices and reasons behind them.

3.1.1 Garmin G1000HTM [11]

The Garmin G100H is a glass avionics suite specifically designed for rotorcrafts. It is an integrated package of flight system mainly made of two display units. One being handling multi-function display (MFD) and the other primary flight display (PFD). It is composed of the following main components:

- GIA 63H – Avionics Unit
- GPS/WAAS – Satellite receiver
- VHF COM – radio communication receiver

VHF NAV – radio navigation unit

- 10.4in GDU – High resolution displays
- GMA 350H – Audio Panel for communication
- GSU 75 ADAHRS – Altitude and Heading reference unit.
- GEA 71H – Engine and Airframe parameter sensing unit
- GTX 33H ES – Transponder for Navigation and radar

3.1.2 Autopilot This is to assist the pilot, in handling degraded visual environment that may accompany a disaster situation, to increase safety and reduce the workload of the pilot.

3.1.3 Datalink The design may be required to operate within a specific airspace. By using datalink, the inherent risk of accident due to collusion as a result of close quarter fleet operation is mitigated. The datalink offers the pilot to see other aircrafts operating within that fleet thus allowing more vehicles to operated safely. In addition, datalink reduced the workload of the pilot.

3.1.4 Enhanced Ground Proximity Warning System (EGPWS) When operating flights near the ground level, Helly-800 uses EGPWS and Terrain Awareness and Warning System. These systems notify the pilot about imminent dangers.

3.1.5 Rain / Ice protection In order Helly-800 to fly at high altitudes, it requires a system to protect against the accumulation of ice within the engine inlets and the other critical parts of the helicopter.

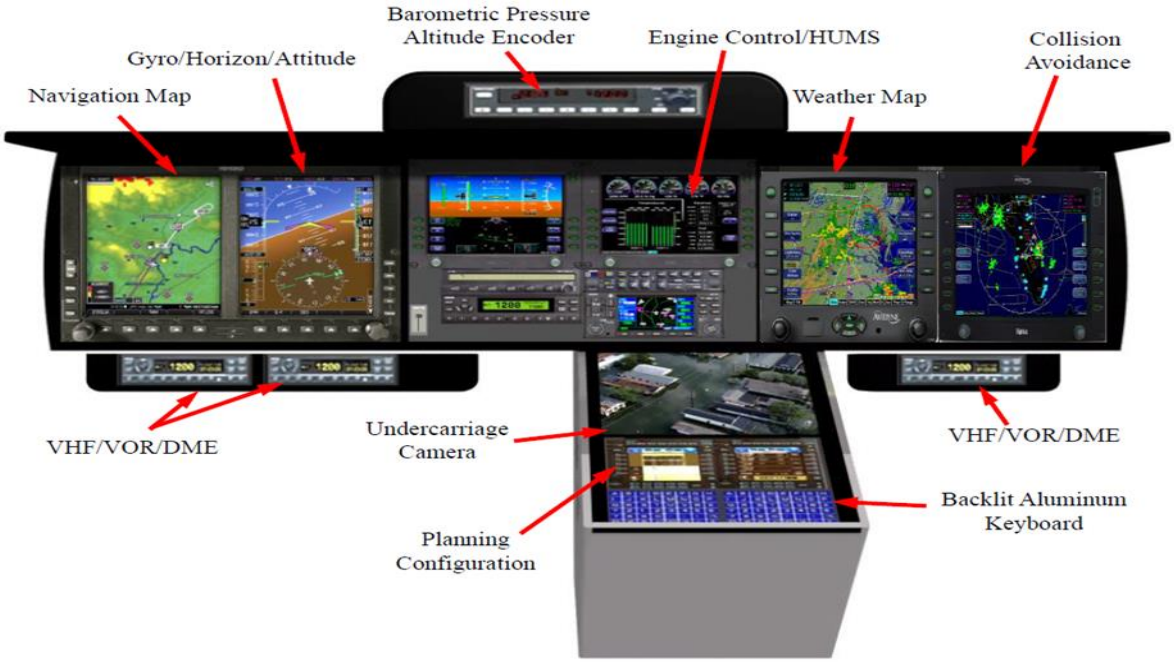

Figure 5: Avionics [13]

4. FLIGHT CONTROLS

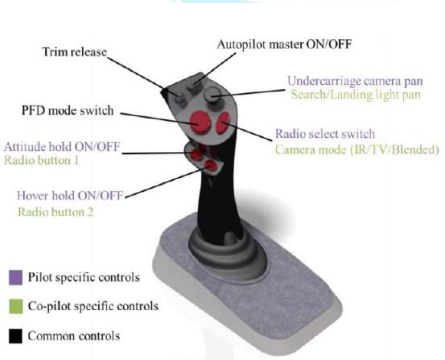

The flight control systems and the pilot control are designed to match the need for the pilot to use them for various flight modes. Helly-800 is equipped with a fly-by-wire architecture with quadruple redundancy which is used to carry control signals to different path around the fuselage to increase safety.

4.1.1 A right handed joystick: this will provide pitch and roll inputs for the forward flight mode, and cyclic control in helicopter mode.

4.1.2 FADECTM ART2: Full Authority Digital Engine Control (FADEC) ART2 is system developed by Safran Electronics & Defense that regulates and monitors the helicopter turbines in order to offer a higher performance range of single or dual channel digital regulation systems. It is made of two parts; one which is a digital computer called Electronic Engine Controller (EEC) or Engine Control unit (ECU), and then its related accessories that monitor all aspects of engine performance. The system has shown to be trustable, reliable and efficient. Thus, it meets our main objective.

4.1.3 A lever and rack mechanism: this will provide up and down collective motion in takeoff and landing mode, fore-aft throttle motion in forward flight mode. This mechanism is also used to reduce the workload of the pilot since there is one pilot.

4.1.4 Conventional foot pedal mechanism: is used for yaw control in all flight modes.

4.1.5 Automatic Flight Control System (AFCS): The design is equipped with AFCS to enhance smooth transition between different flight modes using extensive and continuous control mixing. In case of critical system failure, AFCS follows a preprogrammed failure logic sequence.

The following figure shows and names all the parts of a VTOL vehicle similar to Helly-800 design. It also shows and specified for all subsystems that will be used in the design of Helly-800.

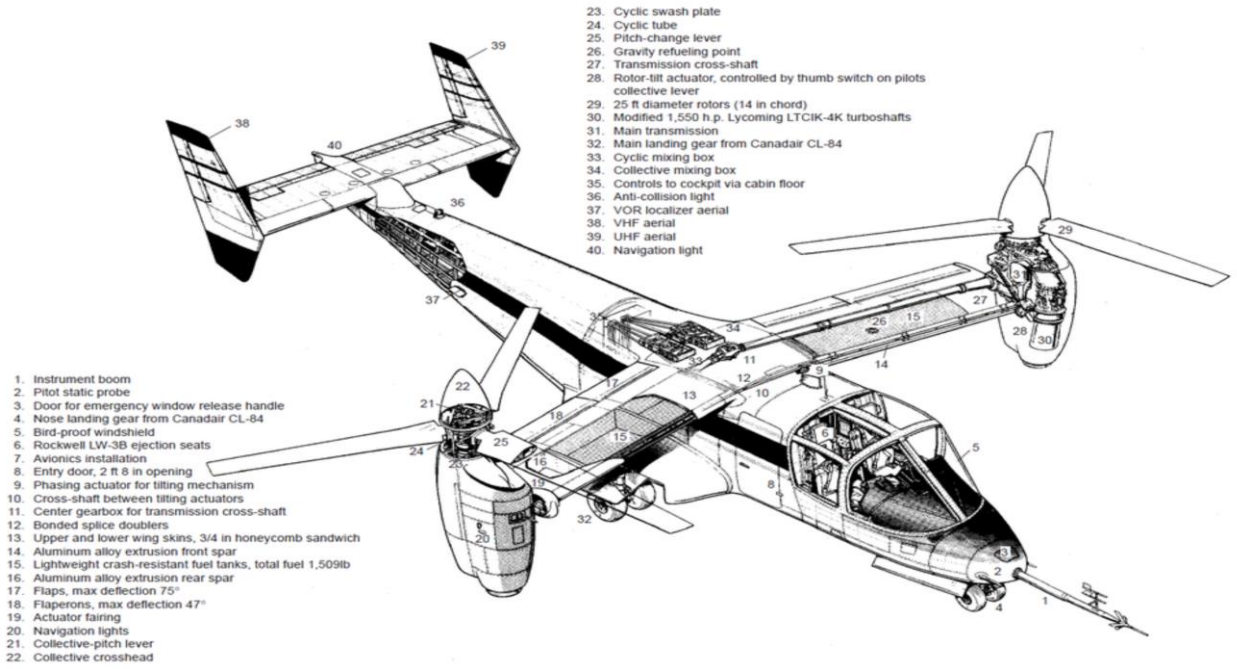

Figure 6: Subsystems and their visuals [14]

Subsystem	**Volume**
Landing gears storage	
Engine	
Fuel tank	
Control surfaces	
Power transmission	

5. COCKPIT SIZING AND ANTHROPOMETRIC DATA

Human size is one of the most importance factor in determining cockpit dimensions. Therefore, the cockpit sizing will be in accordance with anthropometric standards as per the requirement of the project. Anthropometrical characteristics is very important aspect in cockpit sizing by evaluating cockpit reach compatibility to control. We viewed Anthropometric evaluation of cockpit designs paper by Mehmet Burak. [4] This article focuses of turkey population which is considered as Indo-Mediterranean which has a proportion similar to European. [5]

An algorithm is designed to determine a design which finds the lowest seat position possible that allows the pilot to have satisfactory exterior vision. This will give the plot the ability to reach and operate the critical controls. For the anthropometric data, seating position, and visual comfort of the pilot are analyzed.

5.1.1 Seating sizing

Seat sizing is very importance for the pilot's comfort. The minimum distance between the back support of the cushion of the seat or the other fixed structure in front is 66.0 cm, the minimum distance between a seat and the seat of other fixed structure in the front is 17.8 cm, and the minimum vertical projected distance between seat rows or between a seat and any other fixed structure forward of the seat is 7.6 cm. [7] The space around the seat is an importance comfort factor in long hour flights. Table 1 below shows compared cockpit dimensions and anthropometric measurements with the above recommended dimension.

Dimension	Minimum (current)	Minimum (recommended)
A	66.0 cm	71.1 (95%) or 74.7 (99%)

B	17.8 cm	Armrest level 23.0–23.5 Cushion level 21.0
C	7.6 cm	30.5 (95%)
Foot rest	-	35.5
Armrest	-	49.7 (95%) or 58.3 (99%)

Table 1: recommended seat dimensions [4]

Table 2 shows anthropometric results for the standard deviation SD, mean (μ), lower point limit LCL, and upper point limit UCL of measurements for eye distance, eye level, elbow level, stature and arm span. A sample of data was obtained from 100 male helicopter pilot whom their ages were between 24-44 years. The mismatches between anthropometric data and the cockpit dimensions were removed then table 2 was formulated.[4]

Measure	SD	μ	LCL	UCL
Eye distance	2.6	40.6	36.3	44.8
Eye level	2.6	99.6	95.2	104.0
Elbow level	3.2	40.8	35.4	46.2
Stature	4.8	174.6	166.7	182.5
Arm span	3.7	70.7	66.6	76.9

Table 2: Measurement from anthropometric data [1]

5.1.2 Visual comfort sizing

General aviation accident statistics show that instrument meteorological conditions and visual flight rules are major safety hazards. [6] Visual sufficiency of the cockpit design should be done with respect to anthropometric measurements. Location and task of the visual displays are crucial since it determines the posture of the head and the neck. The suitable location of displays from the eyes of the pilot is also major factor in satisfactory posture and visual comfort.

The middle part of the visual field sensitive for tasks such as reading a text and recognizing a face. [10] Therefore the direction of the sight can be altered using combination of movement of eyeballs and the movements of neck and head. The eyes may be raised by 48° and lowered by 66° without head movements. [8] In practice, a part of this range is used. A study by Weston [9] about visual fatigue suggests that the eye movement in downward direction were limited to 24°-27°; beyond that point the head and the neck are inclined forward. In an experiment by Grandjean et al. [10] described group of visual display unit (VDU) operators were given an adjustable workstation and encouraged to set it to their own satisfaction; the preferred visual angle was 9° downwards from the horizontal. Brown and Schaum [11] have also conducted fitting trials on VDU workstations. Their results are reported in coordinate form but it is possible to calculate that the average preferred visual angle was 18° downwards.[7] Burak [7] found out that the preferred zone for vision extends from the horizontal line of sight downwards to an angle of 30° and the optimal line of sight is somewhere in the middle of this zone. Given that some modest degree of neck flexion is acceptable this could be extended a further 15° (see Figure 1).

To prevent eyestrain due to the visual work done extensively close to the eyes, the viewing distance is considered as 35 cm, but between 50 cm to 70 cml is desirable (see figure 1). The figure 1 below combined the above measurements and gives overall view of the proposed system draft.

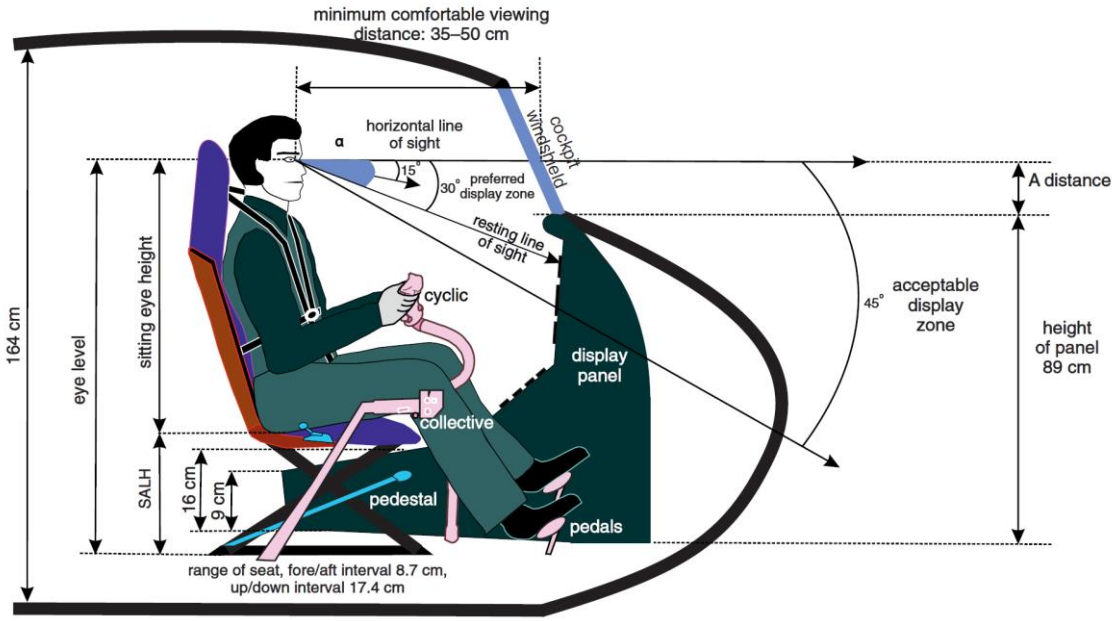

Figure 7: Recommended system draft [1]

6. HELICOPTER SIZING

Combination of the momentum theory and the blade element theory [3] is used to size the helicopter. These methods provide an efficient methodology to determine the weight and sizing of the rotorcraft. To apply these methods, several assumptions and modifications are implemented. First, absence of the tail rotor eliminates the extra power requirements for the tail rotor, and extra weight component due to the tail rotor. In addition, power requirements for the forward flight are calculated similarly to the turbo-prop airplanes.

The formulae used in calculating the weights, in empirical sizing methods for conventional rotorcrafts is modified using the equations from “NASA Design- Analysis of Rotorcraft (NDARC)” and “Helicopter Performance, Stability and Control book, Prouty,R”, [2] to account for the weights of the wing and spinner. These equations are also used to account for the wing related terms such as lift and drag due to the wing and downward force during hovering flight regime. Spinner modifications are also added to decrease hug drag in forward flight condition.

The engine characteristics are also modified in accordance with NDARC engine model. Additional weights are considered to account for the weight of the tiltrotor features such as rotor system and interconnecting drives (see the drawings in the appendix)

Numerical calculations are performed using a code that is based on the NDARC equations, and uses an iterative process starting with the minimum design requirements such as cruise speed of 400 km/h, payload of 250 kg, and a range of 800 km. Additional initial parameters such as figure of merit, propulsive efficiency, transmission efficiency, disk loading, blade and wing aspect ratio, tip speed and number of blades are included.

The following procedure is used in the iterative process for sizing of the helicopter:

1. Payload, range, endurance, and cruise speed are taken as requirement inputs.

2. Number of blades, disk loading, and proprotor blade aspect ratio in hover are takes as inputs. Additional inputs include figure of merit in hover, wing aspect ratio, propulsive efficiency, wing loading, and transmissive efficiency.
3. The first initial guess of gross takeoff weight, GTOW, is decided from the design trends.
4. Using the momentum theory the diameter for the tiltrotor required to hover is calculated given the values of disk loading and initial GTOW.
5. After establishing the blade aspect ratio and diameter, the blade chord is determined.
6. Based on the initial GTOW, figure of merit, disk loading and wing loading, the power required to hover is calculated.
7. The wingspan is determined from the geometric constraints using a selected aspect ratio.
8. Using the values of the power required for the mission and endurance, as well as the information about the specific fuel consumption of the engine, the estimated fuel weight is calculated.
9. Empty weight is obtained as a sum of the individual components weight.
10. The GTOW estimation is performed via an iterative computational process.

Figure 1 shows the schematics of the iterative process used for the sizing and weight calculation.

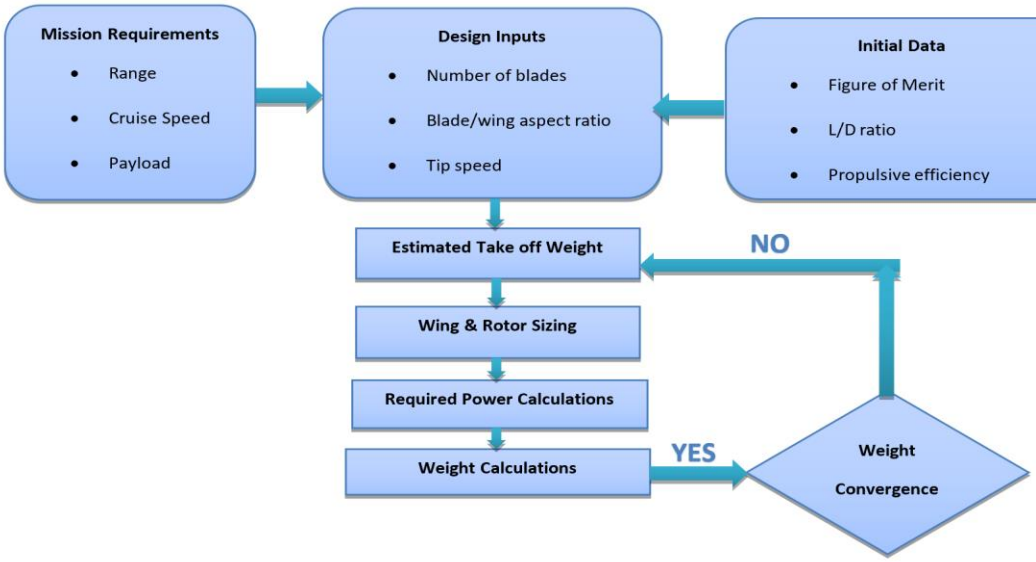

Figure 8: Iterative computational process for weight estimation

Sizing Formulas:

6.1.1 Main rotor group weight:

$$W_R = 1.7 \times {W_G}^{0.342} \times R^{1.58} \times \sigma^{0.63}$$

where W_R is the weight of the main rotor group in kg, R is the radius of the rotor in m, σ rotor solidity, and W_G is the take-off gross weight of our design helicopter in lb.

6.1.2 Power plant group weight:

$$W_T = 0.116 \times HP$$

where W_T is the weight power plant group in kg and HP is the horse power of the engine of the design helicopter. The design will use two engines, PW 210 turboshaft engine, with power output of 1000 Hp each.

6.1.3 Power Plant section group weight:

$$W_{PS} = 0.00155 \times {W_G}^{1.07} \times \omega^{0.54}$$

where W_{PS} is the weight of the power plant section group in kg and ω is disc loading in kg/m^2

6.1.4 Mechanical drive system group weight:

$$W_{PS} = 42.4 \times \left(\frac{HP \times R}{V_T}\right)^{0.763}$$

where V_T is the rotor tip speed in m/s.

6.1.5 Flight control group weight:

$$W_{FC} = 0.0226 \times {W_G}^{0.712} \times {V_C}^{0.653}$$

where W_{FC} the weight of the flight is control group in kg and V_C is the cruise velocity in knots of the design helicopter. From the competitor study, V_C varies between 60 knots and 100 knots therefore V_C is selected as 85 knots to have a relatively fast helicopter to cover the range.

6.1.6 Landing gear group weight:

$$W_{LG} = 0.0475 \times {W_G}^{0.975}$$

6.1.7 Fuselage group weight:

$$W_F = 0.0382 \times {W_G}^{0.598} \times L^{0.942} \times W^{0.453} \times H^{0.295}$$

where W_F is the weight of the fuselage group in lb, L is the length of the fuselage in m, W is the width of the fuselage is m and H is the height of the fuselage in m.

6.1.8 Avionics

Average value of avionics=150 lbs=68.04 kg

6.1.9 Furnishing & equipment

$$W_{eq} = 13\left(\frac{W_G}{1000}\right)^{1.3}$$

7. FINAL WEIGHT ESTIMATION

The total weight estimation is performed using a component weight approach. Correction factor is used to account for the light composite materials, which are used to manufacture wings, fuselage, and empennage. Table below illustrates the estimated weights of the major components and subsytems.

Parameters	Weight (kg)
Wing	315
Rotors	255.7
Fuselage	254.6
Stabilizers	233
Payload	250
Crew	80
Dry weight of the engine	2×161

Fuel	1216
Mechanical drive system	317
Landing gear	146
Power Plant Section Group	93.3
Flight Control Group	214.2
Avionics	67.5
Furnishing & Equipment	95.6
∑Total empty weight	2312
∑Total gross weight	3858

Table 4: Weights of the Components

8. FUEL CONSUMPTION

A suitable engine is selected after a market search, and to estimate fuel consumption for the given minimum range and endurance requirements some calculations are made accordingly;

Minimum endurance 3 hours, minimum range 800 km.

- 2 × Pratt & Whitney Canada PW210A turboshaft engines
- 2 × 1000 HP (for Mechanical Power Class)
- SFC 0.53 $\frac{lb}{hp \times h}$
- Propulsive efficiency, η_{pr} is taken as 0.85.

$$W_{fuel} = SFC \times P_r \times time$$

Available power P_a is taken as engine shaft horsepower

$$P_r = P_a \times \eta_{pr}$$

Then, W_{fuel} is calculated 2703 lb = 1216.3 kg.

Various types of fuel have been selected for the helicopter, the desired or available fuel types can be used under suitable conditions. Preferred fuel types and usage conditions are as follows;

- Primary: JP-4/JP-5/JP-8/Jet A/Jet A1/Jet B/GB6537-94(RP-3)
- Alternate: AVGAS/Jet A,), A1, or JP5 mixture
- Do not use AVGAS containing Tri-Cresyl-Phosphate (TCP)
- Do not use above 4°C (40°F).
- For operations below 4°C (40°F), anti-ice additive required [1]

9. POWER REQUIREMENTS

✓ **For Forward Flight**

An extensive MATLAB code is written to analyze how much power is needed for the helicopter to hover and to fly forward. Power estimation in forward flight is made by using blade element theory in ff: torque and power. The helicopter needs different amounts of power at different forward speeds. Available-power is installed-power what engines provide, and the required-power is how much power is necessary to fly. In the table below, the power values for cruise flight at 400 km/h is found as:

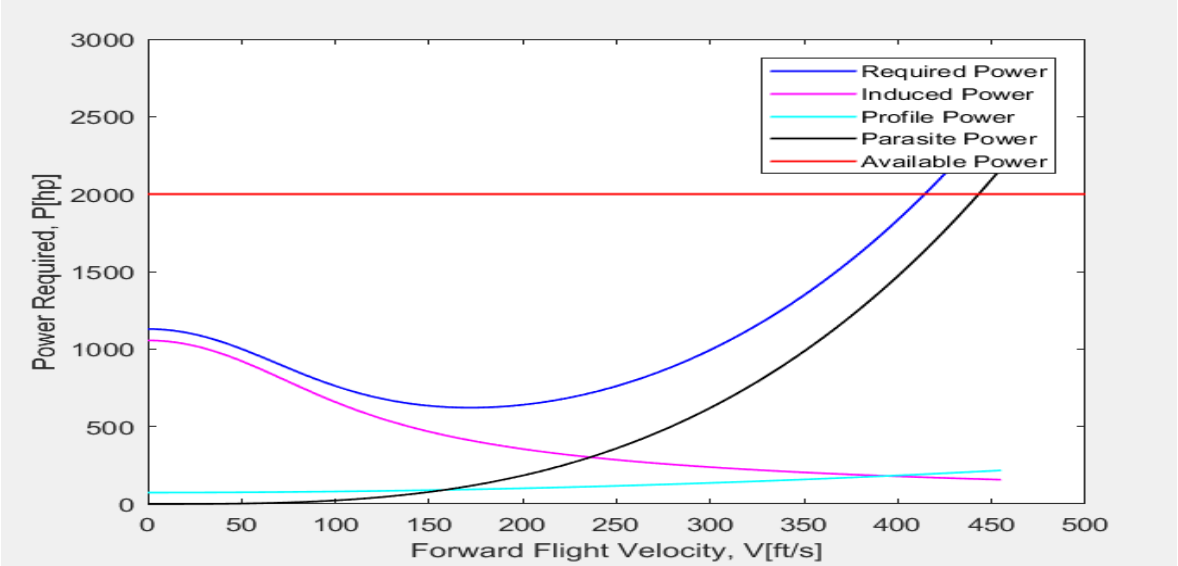

Figure 9: Power against forward flight velocisy

Power Type	Value (hp)
Induced Power	196.1
Profile Power	165.3
Parasite Power	1109
Required Power	1470.4
Available (Installed Power)	2000

Minimum power-required value corresponds to maximum endurance velocity value, V_{Emax}. When a straight line is drawn from the origin, the tangent point to the required-power curve, the velocity corresponds to the speed for maximum range, V_{Rmax}. The maximum speed, V_{max} is the intersection of power-available and power-required curve. Zero velocity simply shows how much power is needed to hover, as it is seen from the graphs, in hover the helicopter needs much more power than other maximum range and endurance modes. Helly-800 is also capable for hovering at low altitudes, by following regulations of FAA flight standards minimum suspension ceiling values can be obtained.

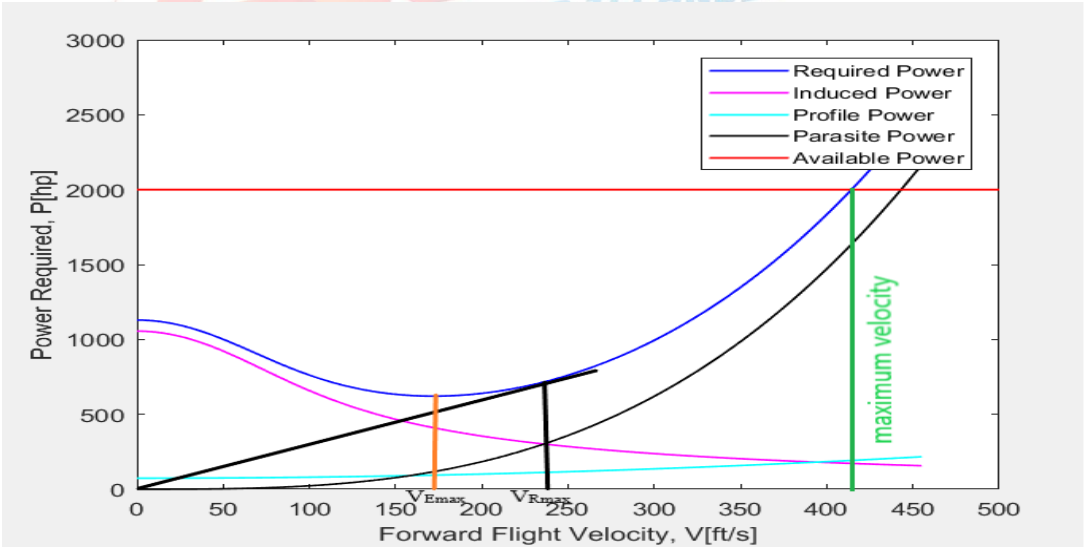

Figure 10:Power required against forward flight velocity

From the power-required/ forward velocity curve the maximum speed is obtained as 415 ft/s which is 455.4 km/h. V_{Emax} and V_{Rmax} are 188.7 km/h, 261.2 km/h.

Performance parameters	**Value**	
Maximum cruising speed [km/h]	455.4	
Maximum Range [km]	1044.8	
Maximum Airborne time [h]	4.24	
Minimum suspension ceiling [m] [11]	**Day**	**Night**
Mountainous local flying areas	243.84	457.20
Mountainous non-local flying areas	304.80	457.20

✓ **For Hover**

Zero velocity shows how much power is needed to hover. Power requirement for hover is 1150 hp as it is seen from the graph.

10. POWER LOSS CALCULATIONS

Main sources of the power losses are:

- Rotor transmission
- Engine nose gearboxes
- Drive system cooling fans
- Transmission-mounted accessories (ex. generators, hydrolic pumps)

10.1.1 The Total Transmission Losses

It can be calculated as:

$$\text{hp}_{\text{trans. loss}} = 0.0025(4000 + \text{Eng. power}) + 0.00875(4000 + \text{Rotor power})$$

Assuming that the engine power is equal to rotor power;

$$\text{hp}_{\text{trans. loss}} = 67.5\ hp$$

10.1.2 Generator and Hydrolic Pump Losses

Assuming typical efficiencies, load (average value is 2200 watts), flow rate(1.3 gpm)and design pressure(average value is 3000 psi) generator and hydrolic pump losses can be calculated.

$$\text{Generator Loss(hp)} = \frac{\text{Load in watts}}{0.75 \times 746}$$

$$\text{Generator Loss(hp)} = 3.93\ \text{hp}$$

$$\text{Hydrolic Pump Loss(hp)} = \frac{(\text{Design pressure, psi}) \times (\text{flow rate, gpm})}{0.80 \times 1714}$$

$$\text{Hydrolic Pump Loss(hp)} = 2.85\ \text{hp}$$

10.1.3 Transmission-Mounted Accessories Loss

To calculate transmission-mounted accessories loss, it is needed to have atmospheric density ratio for standart day condition and for 3500 meter pressure altitude density ratio is taken as 0.7 (Appendix C, Athmospheric Charts [2]):

$$\text{Transmission and accessory Loss(hp)} = \frac{\rho}{\rho_0}(56 + 0.0112 \times hp_{engine})$$

$$\text{Transmission} - \text{mounted accessory Loss(hp)} = 54.88\ hp$$

10.1.4 Engine Installation Loss

Possible engine losses are predicted as follows;

Inlet pressure losses due to duct friction	1-4% of total engine power
Inlet pressure losses due to a particle seperator	3-10% of total engine power
Exhaust back pressure due to friction	0.5-2% of total engine power
Exhaust back pressure due to an infrared suppresor	3-15% of total engine power
Compressor bleed	1-20% of total engine power

10.1.5 Power Loss Due to Parasite and Profile Drag on Helicopter

Using Blade Element Theory in FF total profile and parasite drag power is calculated as 165.3, and 1109 hp for 400 km/h forward speed.

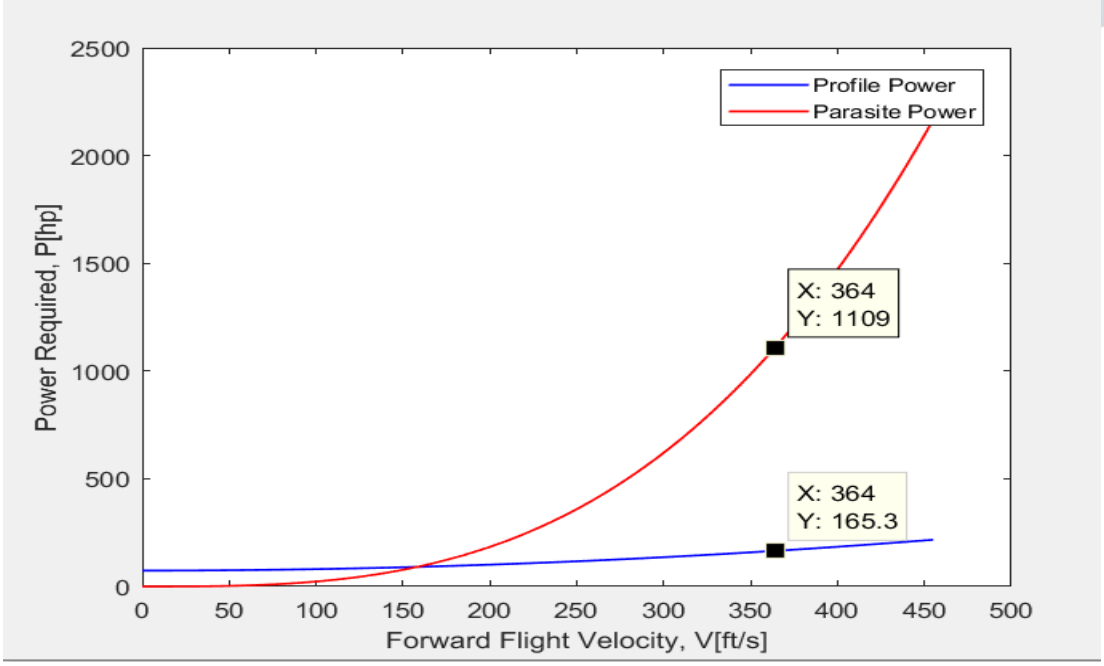

Figure 11: Total power loss prediction is estimation

Total power loss prediction is estimated to be approximately 1445 hp

11. CFD ANALYSIS OF HELLY-800

In the project, the Cfd analysis of the aircraft was done at different velocities and different altitudes. The aim of this was to see the effects of the velocity differences and density differences on the aircraft.

The first analysis was done at cruise speed (111.11 m/s) and at sea level where the air density is 1.225kg/m^3 and the viscosity is 1.7894×10^{-5} kg/m-s.

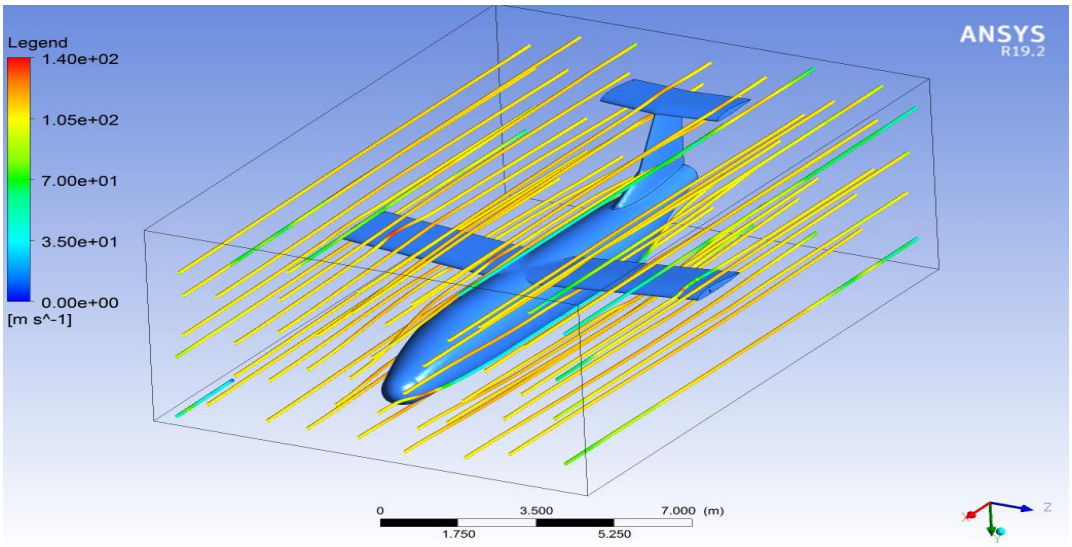

Figure 1: CFD analysis at sea level with 111.11 m/s cruise speed

In the analysis, it was realized that the turbulence was appeared at the horizontal tail and wing. Also, the blue lines of the wing shows that on the some parts of the wing the velocity is equal to zero because of the frictional load. However, it is less enough not to considered.

Moreover, it can be seen that the flow distribution around the wing is smooth and vortex appearance cannot be seen.

In the second analysis, the aircraft, which has 126.5 m/s maximum speed, was analyzed at sea level where the air density is 1.225kg/m^3 and the viscosity is 1.7894×10^{-5} kg/m-s.

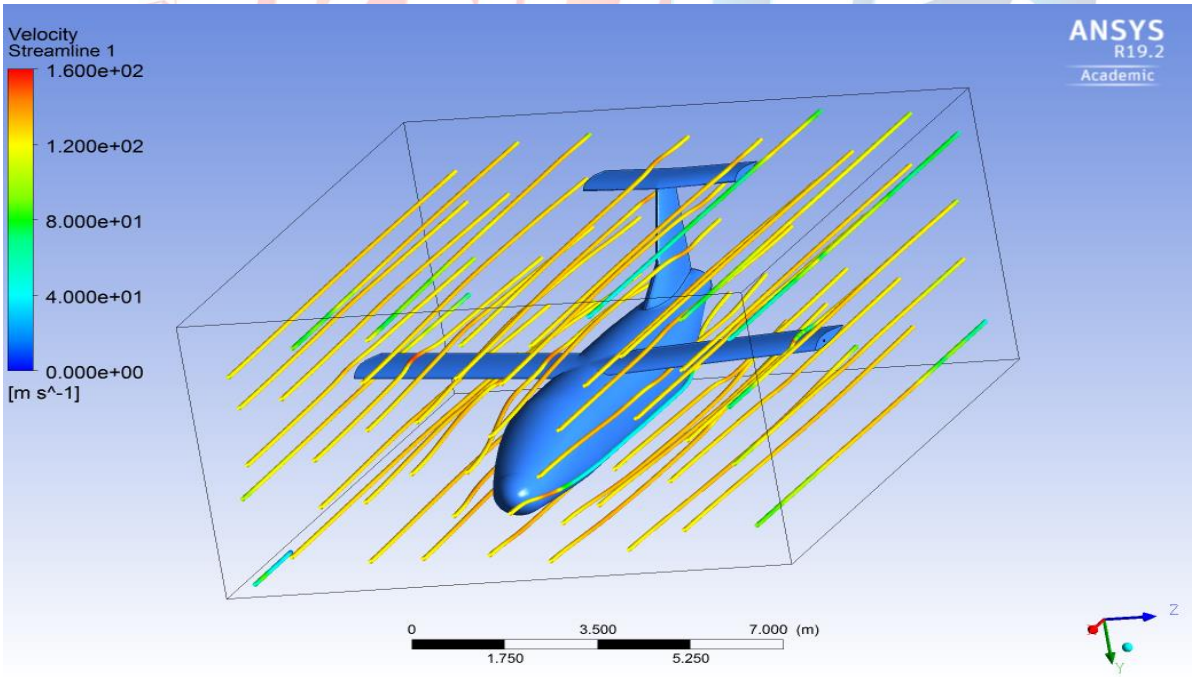

Figure 2: CFD analysis at sea level with 126.5 m/s maximum speed

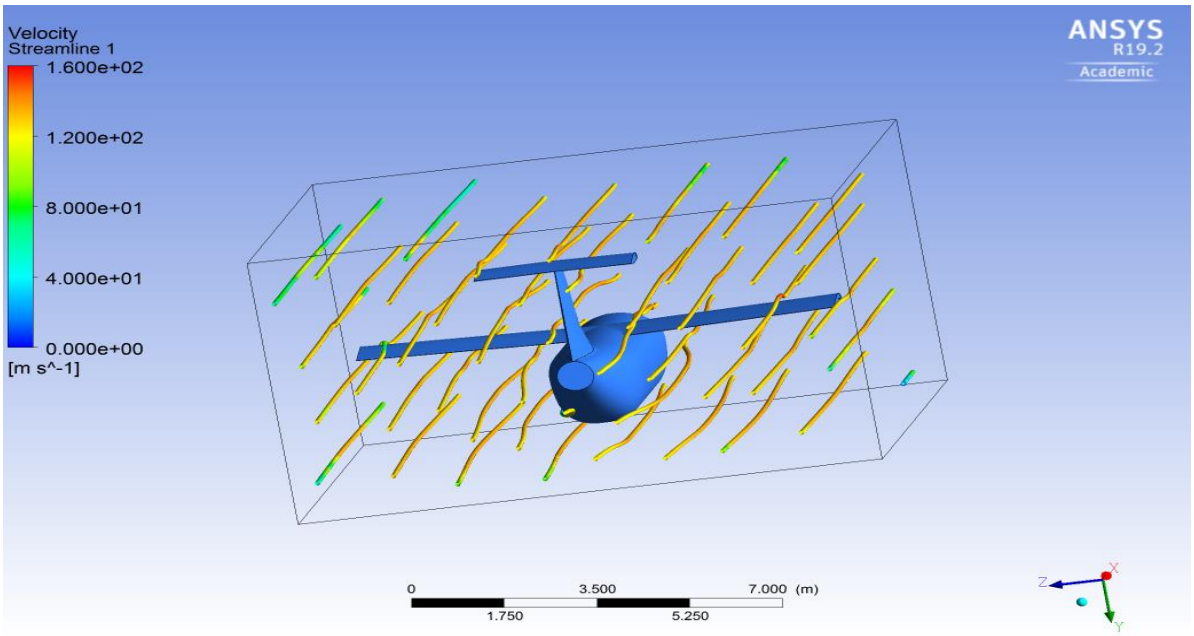

Figure 3: CFD analysis at sea level with 126.5 m/s maximum speed (back side of the aircraft)

In the third analysis, the aircraft, which has 126.5 m/s maximum speed was analyzed at 3500 meter altitude where the air density is 0.864 kg/m^3 and the viscosity is 1.696×10^{-5} kg/m-s.

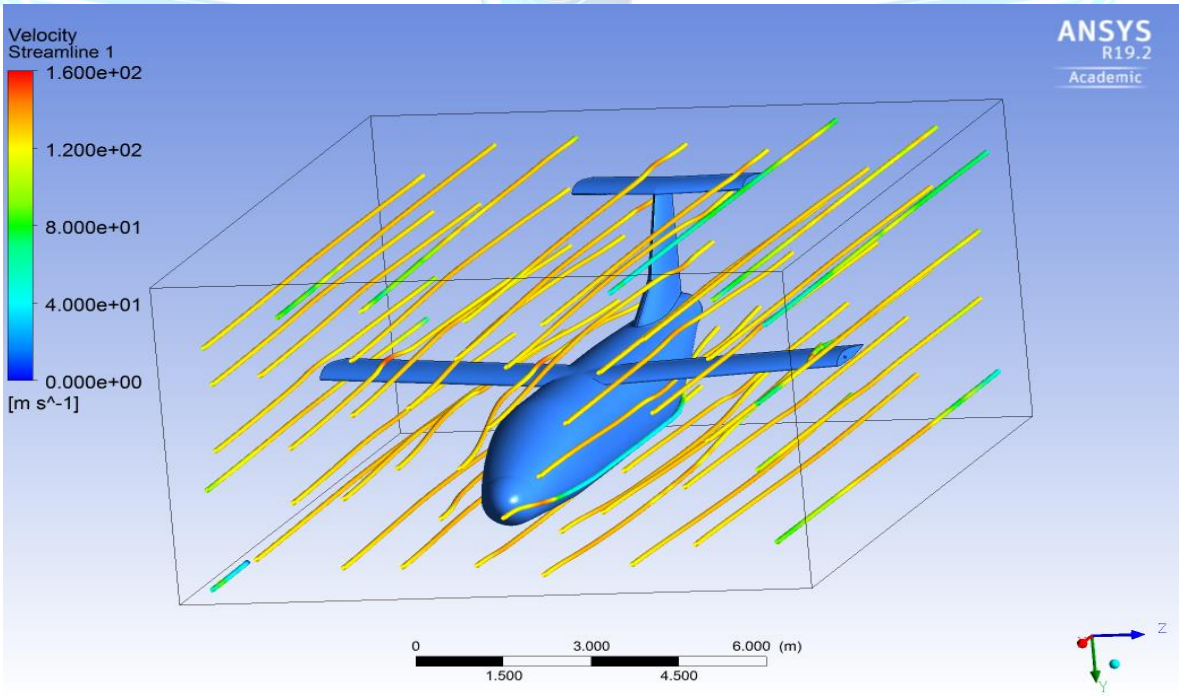

Figure 4: CFD analysis at 3500 m altitude with 126.5 m/s maximum speed

In the fourth analysis, the aircraft, which has 126.5 m/s maximum speed was analyzed at 457 meter altitude where the air density is 1.17217 kg/m^3 and the viscosity is 1.775×10^{-5} kg/m-s.

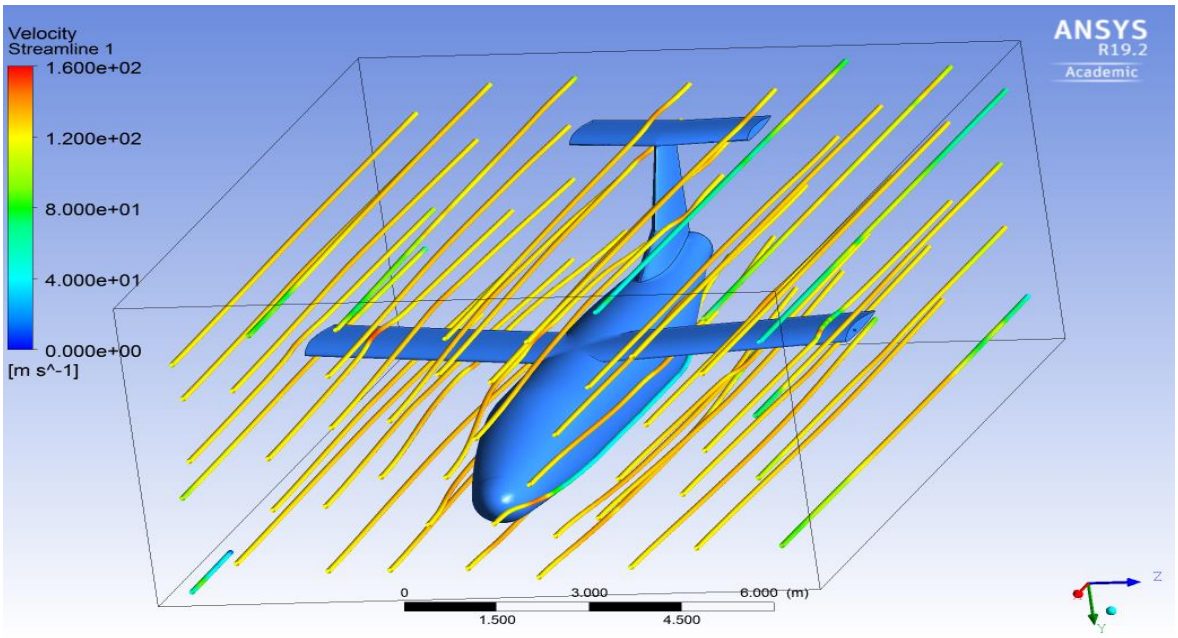

Figure 5: CFD analysis at 457 m/s with 126.5 m/s maximum velocity

In the analyses, the velocity and altitude change doesn't affect the flow distribution through the helicopter significantly. It can be realized that the flow through the helicopter is moving smoothly and there is no negative aerodynamic effects on whole helicopter.

Structural Analysis

In the structural analysis, the weight of the components of the helicopter, the thrust distribution which was generated by the rotors and wings and the dynamic pressure values were defined on the structure. To have safer results, the total pressure was multiplied by safety factor, n=2.

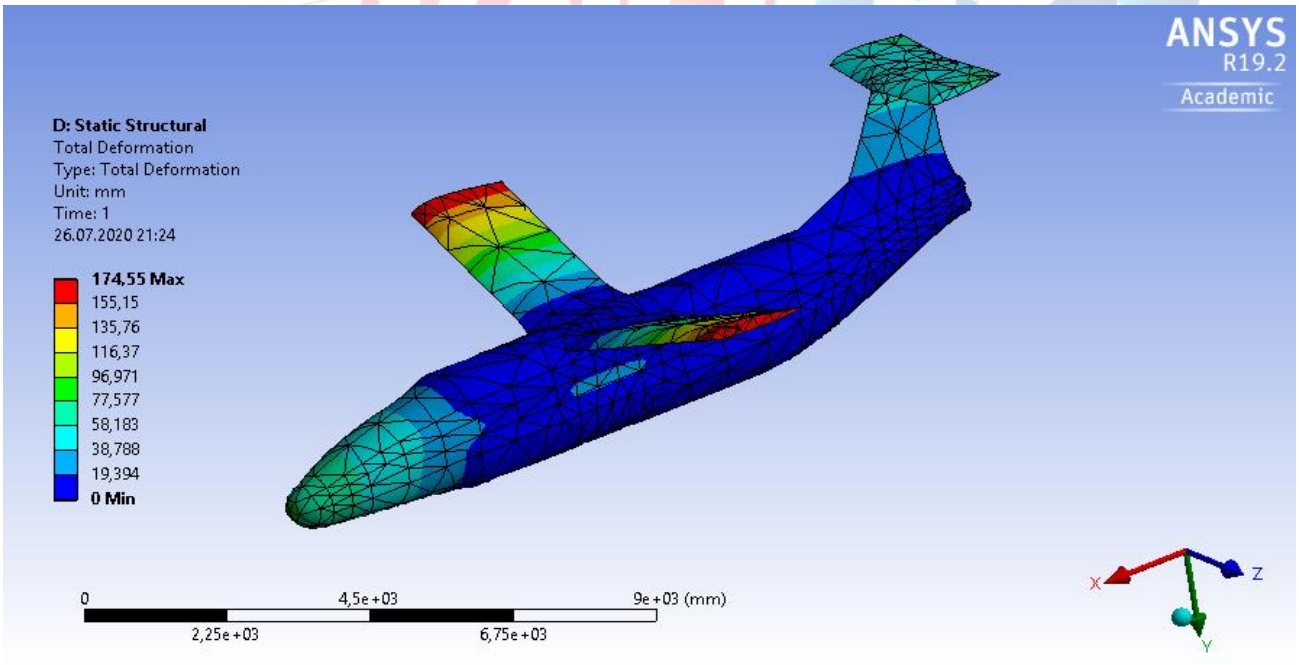

Figure 6: Structural analysis: Total deformation results

In the analysis, it was realized that the most deflection is on the wing tip, 0.174 m. However, for the simple design of the aircraft, the deflection is acceptable. The reason of this is that the wings of the helicopter

doesn’t include the structural supports (ribs, spars, stabilizers) at this step of the design. In the following procedures of the helicopter design, the spar, rib designs can help to optimize the deformation in the wing tips. For this ANSYS analyses the results are acceptable and it can be improved by replacing the structural skeletons inside fuselage and wings.

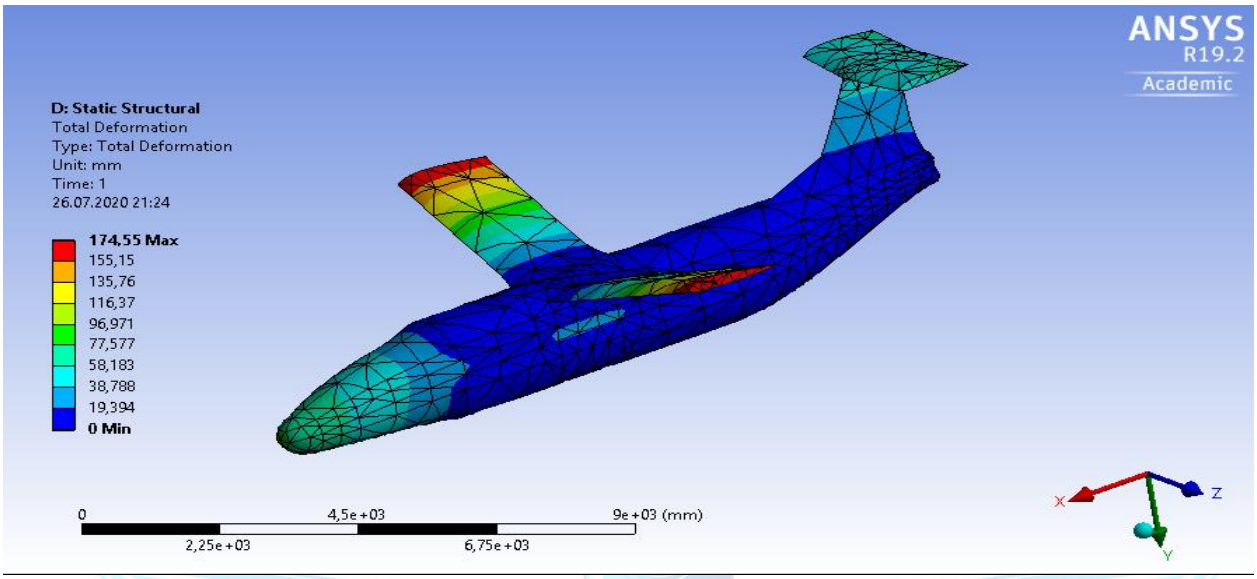

Figure 7: Structural analysis: equivalent stress results

In the equivalent stress results, it can be seen that the stress is distributed on the aircraft smoothly. It shows that the designed aircraft can carry the forces which applied sufficiently.

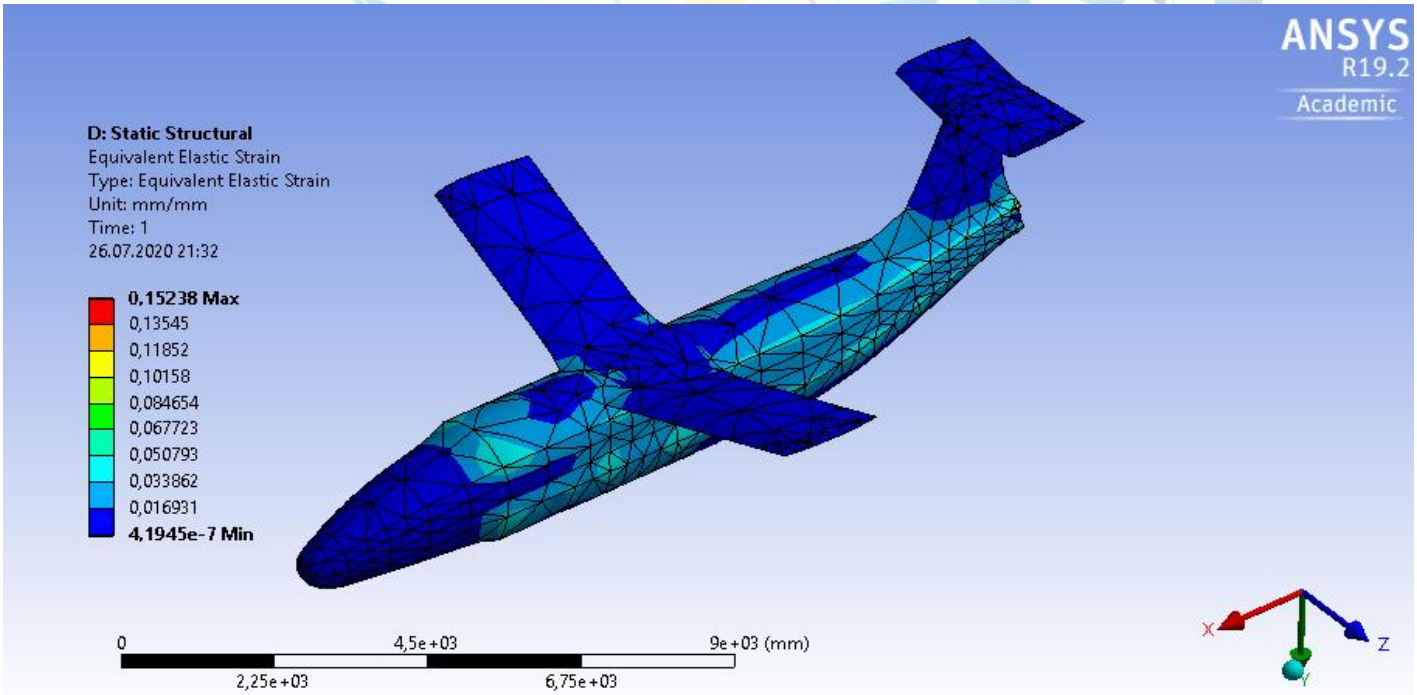

Figure 7: Structural analysis: equivalent stress results

Also, the equivalent elastic strain results are approximately 0.033-0.05 on the aircraft body and it is effective for the designed aircraft.

12. OPTIMIZATION

12.1.1 Weight Optimization

From the MATLAB code which is attached, it is observed that as the disc loading increases, the gross take-off weight of the helicopter decreases. Therefore, using different disk loadings from competitors, the gross takeoff weight is optimized. Hence, the value of disc loading selected is 68.35 kg/m2 (14 lb/ft2) because this disc loading value resulted to the lighter weight. Therefore, our estimated gross take-off weight is taken as W_G =3858 kg. This makes Helly-800 to be light helicopter for this mission. In addition, the main rotor diameter is optimized in the same optimization code and its value is found to be 3.96 meters (13 ft).

12.1.2 Power Optimization

The power required for the hover condition is optimized using different disk loadings too. The power plant is chosen as PW210A turboshaft engine 2x1000 HP, thus the power required for the hover condition can be easily satisfied and the remaining extra power is available for use in other flight conditions and other power required by the helicopter. As it is seen on the graph (Power vs forward speed), the maximum speed that the design helicopter can fly is approximately 455 km/h. This limitation is due to the available power from the engine. From the design requirements by TEKNOFEST, the cruise speed should be more than 400 km/h hence Helly-800 design can sustain this requirement.

12.1.3 Aerodynamic Optimization

11.2.1 Airfoil Selection

Firstly, blades were divided into segments. To determine how many of them are needed and what ranges are required, maximum and minimum Reynold's Number were calculated and then they were arranged with respect to the information provided by the website airfoiltools.com. Reynold's Number calculation was done with formula of

$$Re = \frac{\rho v c}{\mu}$$

where μ: dynamic viscosity=$1.789 \times 10^{-5} \frac{kgm}{s}$, $\rho: density = 1.225 \frac{kg}{m^3}$, $v: speed \frac{m}{s}$, $c: chord\ length[m]$=0.2524 m

Maximum speed is V_{tip}=213.36 m/s. So, using maximum radius, rotational speed of the main rotor, Ω can be found as

$$\Omega = \frac{\text{Vtip}}{\text{R}} = \frac{213.36\text{m/s}}{3.9\,m} = \frac{54.71}{s} = 343.74\,rad/s$$

Since there is a cut-out at the root of the blade with a 5 percent, minimum radius, the closest blade location to the hub, *R*min= 0.198m. Thus, minimum speed can be calculated as

$$v_{min=} = \Omega \text{R}_{min} = 54.71 \times 0.198 = 10.83 \frac{m}{s}$$

Then, maximum and minimum Reynold's Numbers were calculated by

$$Re_{max} = \frac{1.225 \times 213.36 \times 0.2524}{1.789 \times 10^{-5}} = 3.688 \times 10^6$$

$$Re_{min} = \frac{1.225 \times 10.83 \times 0.2524}{1.789 \times 10^{-5}} = 187173.153$$

After that, defining non dimesional radius r, nondimensional coefficient of radius R varying from 0.05 to 1 and indicating the location of the process, segment boundaries were determined in terms of r with respect to

the information given in the website. Having calculated where Reynold's Numbers 200000, 500000, 1×10^6corresponds in r, segments were divided as

$$1^{st}\ Segment = 0.05\text{: r: } 0.076\ , \mathrm{Re} = 100000$$

$$2^{nd}\ Segment = 0.76\text{: r: } 0.188\ , \mathrm{Re} = 200000$$

$$3^{rd}\ Segment = 0.188\text{: r: } 0.237\ , \mathrm{Re} = 500000$$

$$4^{th}\ Segment = 0.237\text{: r: } 1\ , \mathrm{Re} = 1000000$$

Desired data for the airfoils NACA0012 and VR-7 was obtained in each segment for 3 different angles of attacks α=0°,5°,10° seperately from the website. After that, in each segment, data obtained from 3 different angle of attacks was averaged and required characteristic parameters were found.
For the data of $CL\alpha$, slope of CL vs α curve was calculated. Moreover, drag coefficient, CD were chosen at the angle of attack where CL=0 to have the form drag coefficient, C_{D0}.

Data for VR-7 Airfoil

- **First Segment**

$$\boldsymbol{\alpha}\mathbf{=0°}\quad C_{L_\alpha} = \frac{C_{L_2} - C_{L_1}}{\alpha_2 - \alpha_1} = \frac{0.0651 - 0}{0.25} = 0.2604$$

$$\boldsymbol{\alpha}\mathbf{=5°}\quad C_{L_\alpha} = \frac{C_{L_2} - C_{L_1}}{\alpha_2 - \alpha_1} = \frac{0.6141 - 0.5953}{0.25} = 0.0752$$

$$\boldsymbol{\alpha}\mathbf{=10°}\ C_{L_\alpha} = \frac{C_{L_2} - C_{L_1}}{\alpha_2 - \alpha_1} = \frac{0.9661 - 0.9598}{0.25} = 0.0252$$

$$C_{L_\alpha} = \frac{0.2604 + 0.0752 + 0.0252}{3} = 0.1203, C_{D_0}\text{=}0.0169$$

- **Second Segment**

$$\boldsymbol{\alpha}\mathbf{=0°}\text{:}C_{L_\alpha} = \frac{C_{L_2} - C_{L_1}}{\alpha_2 - \alpha_1} = \frac{0.0350 - 0}{0.25} = 0.1400$$

$$\boldsymbol{\alpha}\mathbf{=5°}\text{:}\ C_{L_\alpha} = \frac{C_{L_2} - C_{L_1}}{\alpha_2 - \alpha_1} = \frac{0.6195 - 0.5990}{0.25} = 0.0820$$

$$\boldsymbol{\alpha}\mathbf{=10°}\text{:}C_{L_\alpha} = \frac{C_{L_2} - C_{L_1}}{\alpha_2 - \alpha_1} = \frac{1.0067 - 0.9882}{0.25} = 0.0740$$

$$C_{L_\alpha} = \frac{0.1400 + 0.0820 + 0.0740}{3} = 0.0990, C_{D_0}\text{=}0.0102$$

- **Third Segment**

$$\boldsymbol{\alpha}\mathbf{=0°}C_{L_\alpha} = \frac{C_{L_2} - C_{L_1}}{\alpha_2 - \alpha_1} = \frac{0.0259 - 0}{0.25} = 0.1036$$

$$\boldsymbol{\alpha}\mathbf{=5°}\quad C_{L_\alpha} = \frac{C_{L_2} - C_{L_1}}{\alpha_2 - \alpha_1} = \frac{0.6275 - 0.5904}{0.25} = 0.1484$$

$$\boldsymbol{\alpha}=\mathbf{10}^\circ\ C_{L_\alpha} = \frac{C_{L_2}-C_{L_1}}{\alpha_2-\alpha_1} = \frac{1.0417-1.0224}{0.25} = 0.0772$$

$$C_{L_\alpha} = \frac{0.1036 + 0.1484 + 0.0772}{3} = 0.1097, C_{D_0}=0.0062$$

- **Fourth Segment**

$$\boldsymbol{\alpha}=\mathbf{0}^\circ\ \ C_{L_\alpha} = \frac{C_{L_2}-C_{L_1}}{\alpha_2-\alpha_1} = \frac{0.0269-0}{0.25} = 0.1076$$

$$\boldsymbol{\alpha}=\mathbf{5}^\circ\ \ C_{L_\alpha} = \frac{C_{L_2}-C_{L_1}}{\alpha_2-\alpha_1} = \frac{0.5572-0.5213}{0.25} = 0.1436$$

$$\boldsymbol{\alpha}=\mathbf{10}^\circ\ C_{L_\alpha} = \frac{C_{L_2}-C_{L_1}}{\alpha_2-\alpha_1} = \frac{1.0808-1.0591}{0.25} = 0.0868$$

$$C_{L_\alpha} = \frac{0.1076 + 0.1436 + 0.0868}{3} = 0.1127, C_{D_0}=0.0054$$

Data for NACA0012 Airfoil

- **First Segment**

$$\boldsymbol{\alpha}=\mathbf{0}^\circ\ \ C_{L_\alpha} = \frac{C_{L_2}-C_{L_1}}{\alpha_2-\alpha_1} = \frac{0.0211-(-0.015)}{0.25} = 0.0944$$

$$\boldsymbol{\alpha}=\mathbf{5}^\circ\ \ C_{L_\alpha} = \frac{C_{L_2}-C_{L_1}}{\alpha_2-\alpha_1} = \frac{0.8388-0.8186}{0.25} = 0.0808$$

$$\boldsymbol{\alpha}=\mathbf{10}^\circ\ C_{L_\alpha} = \frac{C_{L_2}-C_{L_1}}{\alpha_2-\alpha_1} = \frac{0.1903-0.1827}{0.25} = 0.0304$$

$$C_{L_\alpha} = \frac{0.0944 + 0.0808 + 0.0304}{3} = 0.0685, C_{D_0}=0.0200$$

- **Second Segment**

$$\boldsymbol{\alpha}=\mathbf{0}^\circ: C_{L_\alpha} = \frac{C_{L_2}-C_{L_1}}{\alpha_2-\alpha_1} = \frac{0.0356-(-0.0120)}{0.25} = 0.1904$$

$$\boldsymbol{\alpha}=\mathbf{5}^\circ\ \ C_{L_\alpha} = \frac{C_{L_2}-C_{L_1}}{\alpha_2-\alpha_1} = \frac{0.8906-0.8664}{0.25} = 0.0968$$

$$\boldsymbol{\alpha}=\mathbf{10}^\circ\ C_{L_\alpha} = \frac{C_{L_2}-C_{L_1}}{\alpha_2-\alpha_1} = \frac{0.1768-0.1640}{0.25} = 0.0512$$

$$C_{L_\alpha} = \frac{0.1904 + 0.0968 + 0.05123}{3} = 0.1128, C_{D_0}=0.0150$$

- **Third Segment**

$$\boldsymbol{\alpha}=\mathbf{0}^\circ\ \ C_{L_\alpha} = \frac{C_{L_2}-C_{L_1}}{\alpha_2-\alpha_1} = \frac{0.0213-(-0.0048)}{0.25} = 0.1044$$

$$\boldsymbol{\alpha}=\mathbf{5}^\circ \quad C_{L_\alpha} = \frac{C_{L_2} - C_{L_1}}{\alpha_2 - \alpha_1} = \frac{0.8740 - 0.8502}{0.25} = 0.0952$$

$$\boldsymbol{\alpha}=\mathbf{10}^\circ \quad C_{L_\alpha} = \frac{C_{L_2} - C_{L_1}}{\alpha_2 - \alpha_1} = \frac{1.2190 - 1.2073}{0.25} = 0.0468$$

$$C_{L_\alpha} = \frac{0.1044 + 0.0952 + 0.0468}{3} = 0.0821, C_{D_0} = 0.0108$$

- **Fourth Segment**

$$\boldsymbol{\alpha}=\mathbf{0}^\circ \quad C_{L_\alpha} = \frac{C_{L_2} - C_{L_1}}{\alpha_2 - \alpha_1} = \frac{0.0160 - (-0.0111)}{0.25} = 0.1084$$

$$\boldsymbol{\alpha}=\mathbf{5}^\circ \quad C_{L_\alpha} = \frac{C_{L_2} - C_{L_1}}{\alpha_2 - \alpha_1} = \frac{0.8856 - 0.8625}{0.25} = 0.1436$$

$$\boldsymbol{\alpha}=\mathbf{10}^\circ \quad C_{L_\alpha} = \frac{C_{L_2} - C_{L_1}}{\alpha_2 - \alpha_1} = \frac{1.2780 - 1.2624}{0.25} = 0.0868$$

$$C_{L_\alpha} = \frac{0.1084 + 0.0924 + 0.0624}{3} = 0.0877, C_{D_0} = 0.0090$$

Thrust coefficient CT and induce power coefficient Cp_i are eliminated by integrating the incremental coefficients along the blade span.
In order to calculate coefficient of thrust and induce power coefficient, the increment coefficients along the blade span was calculated and integrated over the span. Since blade was divided into four segments, CT and Cp_i are needed to calculate in each segment seperately and then summed them up to get total coefficient of thrust and induce power coefficient which is known as Euler's method. However, there are other parameters to be calculated before calculating the coefficients of thrust and induce power.

$$Tangential\ velocity: U_T = \Omega \times \mathrm{r} \times \mathrm{R}$$

$$Perpendicular\ velocity: U_P = \mathrm{v}_i = \sqrt{\frac{T}{\rho A^2}}$$

$$\phi = \frac{U_P}{U_T},\ \mathrm{c}=0.2524\ mm, R=396\ mm,\ d\mathrm{r}=0.001$$

$$Inflow\ ratio\ \lambda = \phi \times \mathrm{r}$$

$$d_{C_T} = \frac{1}{2}\sigma C_L r^2 dr \qquad d_{C_{Pi}} = \frac{1}{2}\sigma(\phi C_L)\mathrm{r}^3 dr = \lambda d_{C_T}$$

$$C_{Pi} = \lambda d_{C_T}$$

In order to calculate coefficient of thrust, thrust (T), density (ρ), area (A), and square of tip velocity is needed. Where

$$\mathrm{T} = \mathrm{W} = 3857 \times 9.81 = 37837.17\ \mathrm{N}$$

$$\mathrm{A} = \pi \times \mathrm{R}^2 = 49.26\ \mathrm{m}^2$$

$$C_T = \frac{T}{\rho \times A \times {V_{tip}}^2} = \frac{37837.17}{1.225 \times 49.26 \times 213.36^2} = 0.01377$$

$$Induced\ Power\ P_i = C_{p_i}\rho A(\Omega R)^3$$

$$Profile\ Power\ P_0 = C_{p_0}\rho A(\Omega R)^3$$

$$Total\ Power\ P_{TOT} = kP_i + P_0\ where\ correction\ factor\ k = 1.15$$

$$Figure\ of\ Merit\ FM = \frac{P_i}{P_{TOT}}$$

VR7					NACA0012				
T,N	P_0,W	P_i,W	P_{TOT},W	FM	T,N	P_0, W	P_i,W	P_{TOT},W	FM
37837.17	4415	2.26×10^6	2.64×10^6	0.8551	37837.17	4412	1.77×10^6	2.08×10^6	0.8511

For the HELLY-800 design helicopter it is decided to use VR-7 airfoil. The airfoil has good performance qualities on terms of our design requirements. After observing the coefficient of lift vs the coefficient of drag curve, together with the coefficient of lift vs angle of attack graph; we see the airfoil is more suitable for our design. [12] The airfoil has a high maximum lift coefficient as seen from the graph on airfoil tools (website), it also results in higher figure of merit compared to symmetric NACA 4 digit airfoil NACA0012. The following graphs show the same. This means our airfoil yields a rotor with lower solidity and hence a lighter weight. Moreover, it allows the flight at a higher rotor thrust and under higher maneuver load factors.

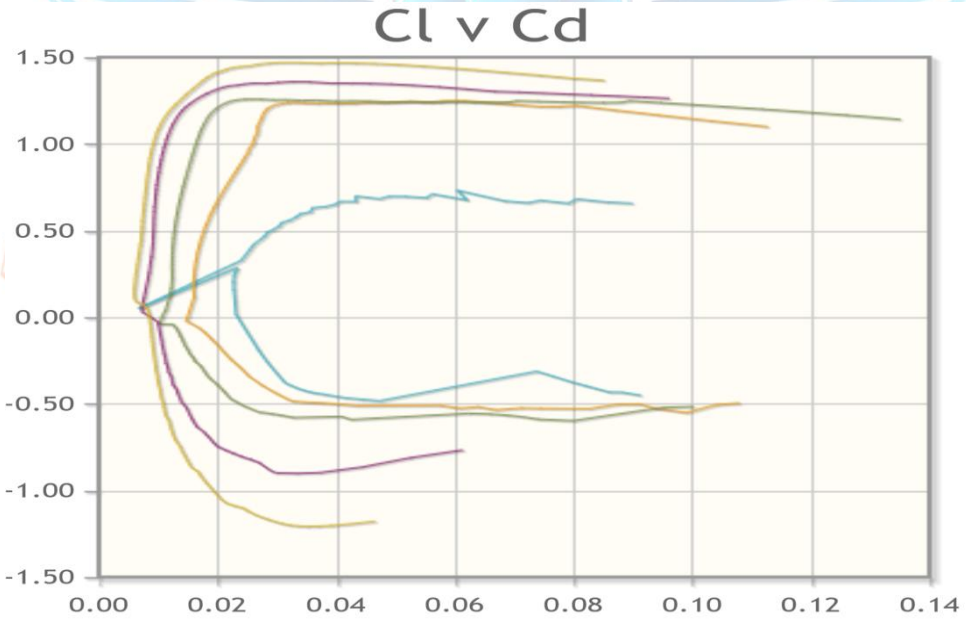

Figure 12: A graph of coefficient of lift C_l vs coefficient of drag C_d for VR-7 [12]

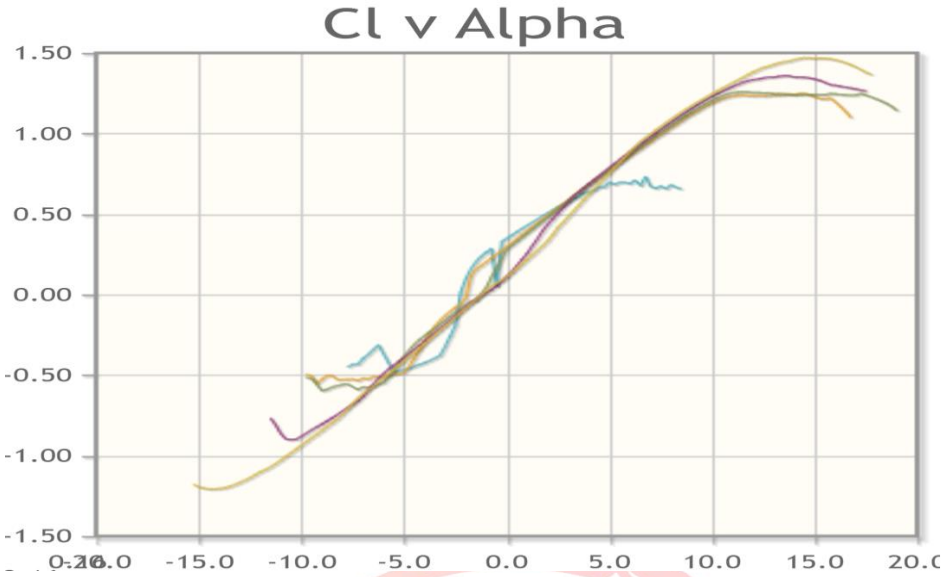

Figure 13: A graph of coefficient of lift C_l vs angle of attack, α for VR-7 [12]

11.2.2 Blade tip design

Blade tips encounter the highest dynamic pressure and highest Mach numbers, and produce strong tip vortices. Blade tip design has a strong effect on the rotor performance. Blade planform effect the lift distribution and, therefore, rotor performance. Small amount of taper over the blade tip region helps to improve the figure of merit. Large amount of taper does NOT give the benefits. Maximum figure of merit can be obtained by using a combination of blade taper and twist. A 2:1 taper over the tip regions can be considered optimal at the initial design stages. With varying sweep angle- sweep angle can be chosen to maintain the incident Mach number (normal to the leading edge) constant. Here is a graph showing the effect of taper on figure of merit.

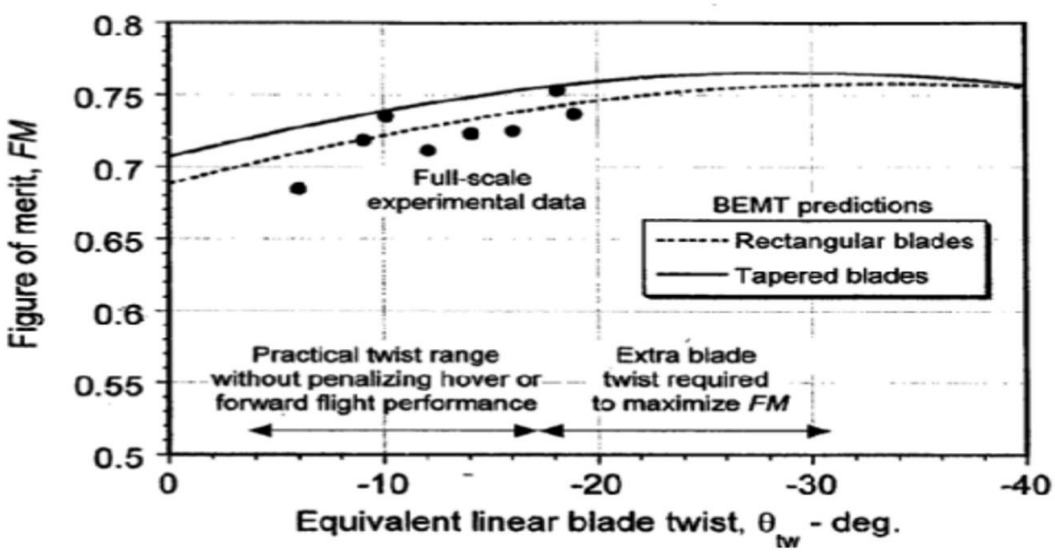

Figure : Figure of merit, FM vs equivalent linear blade twist θ_{tw} in degrees [3]

We therefore consider the parabolic swept tip which ensures this. Below is an illustration of this kind of blade tip. From the above graph we also selected a negative blade twist of 10^0. This blade twist helps to improve the figure of merit making our helicopter efficient during hover.

13. IMAGES

Figure : image showing forward flighht condition

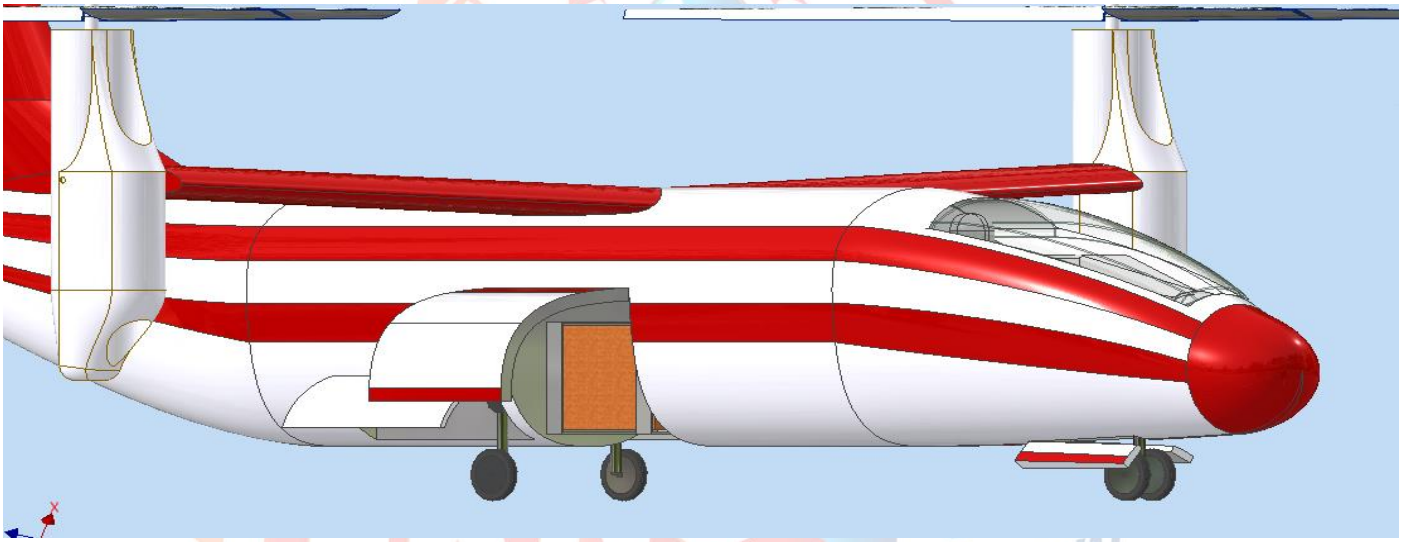

Figure : cargo loarding senario

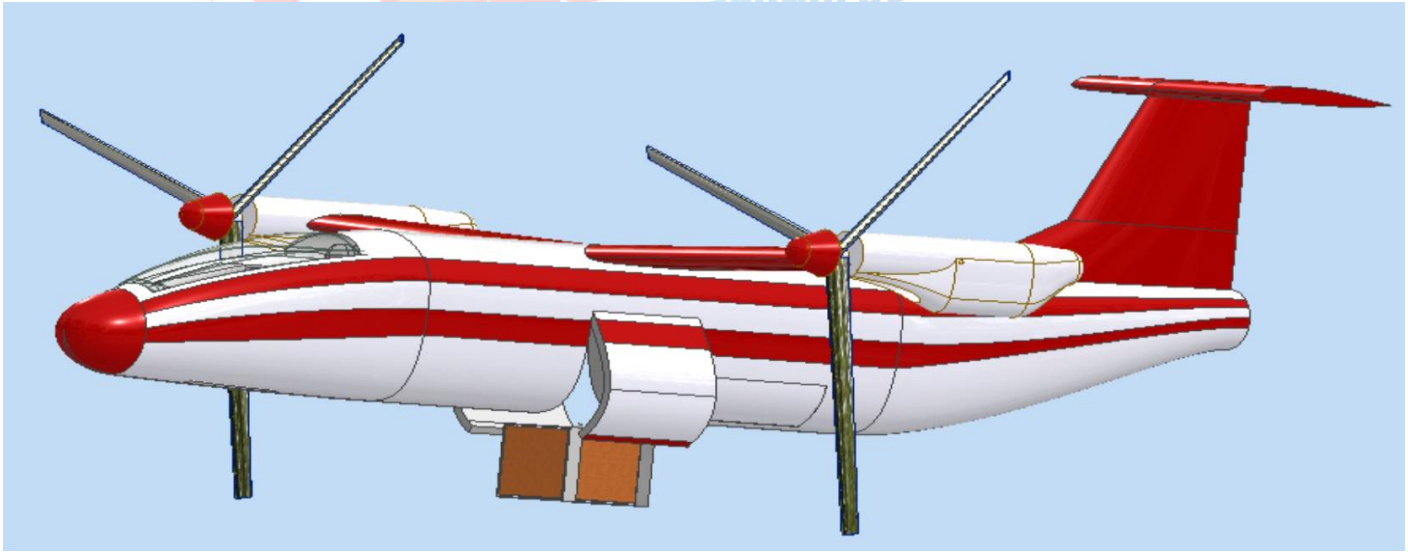

Figure : argo releasing senario

Figure : Takeoff and landing senario

14. CHANGES

In the previous report, the first report, the helicopter's landing gear was the retractable skids. However, this type of landing gear makes it impossible to taxi to the hangar. Therefore, the landing gear type is modified to the retractable landing gear. Moreover, the variable diameter rotor concept, which was mentioned in first report, is replaced with a fixed rotor diameter because of the additional weight, complexity, and increased pilot workload. In addition, the pulley system as cargo unloading mechanism is replaced with a parachute, which allows to reduce time required to deliver cargo. It is opted for that the aircraft performs a fly by and the cargo is released with an attached parachute. This way mission time is reduced as well.

This report is an add on to the previous report which is interim report. There are no changes done at this stage when compared to the interim report.

REFERENCES

1. EASA Type Certificate Holder, *Sikorsky Aircraft Corporation*, Jan 2020.
2. Prouty, Raymond W. (2002) Helicopter Performance, Stability and Control.
3. ohnson, W. (2013). Rotorcraft aeromechanics. Cambridge, U.K: Cambridge University Press.
4. Şenol, M. (2016). Anthropometric evaluation of cockpit designs. International Journal Of Occupational Safety And Ergonomics, 22(2), 246-256.
5. Barli O, Elmali D, Midilli R, et al. Anthropometry of male and female children in creches in Turkey. Coll Antrop. 2005;29(1):45–51.
6. Goh J, Wiegmann D. Human factors analysis of accidents involving visual flight rules flight into adverse weather. J Aviat Spac Envir Med. 2002;73(8):817–822.
7. Pheasant S. Body space, anthropometry, ergonomics and design of work. London: Taylor & Francis; 1986.

8. Taylor JH. Vision in bioastronautics data book. Paker JT, West VR, editors. Washington, DC: NASA; 1973.

9. Weston HC. Visual fatigue with special reference to lighting. In: Floyd WF, Wleford AT, editors. Symposium on Fatigue. London: Lewis; 1953. p. 117–135.

10. Grandjean E, Hunting W, Nishiyama K. Preferred VDT workstation settings, body posture and physical impairments. Appl Ergon. 1984;15:99–104.

11. Brown CR, Schaum DL. User-adjusted VDU parameters. In: Grandjean E, Vigliani E, editors. Ergonomic aspects of visual display terminals. Proceedings; International Workshop. Milan; 1980.

12. Airfoil Tools. (2020). Retrieved 16 April 2020, from http://airfoiltools.com/

13. Weiner, E. & e.d (2013). Heli Executive Summary. Retrieved 20 July 2020, from https://vtol.org/files/dmfile/UMDExecutiveSummary2.pdf

14. Bell XV-15. (2020). Retrieved 20 July 2020, from https://thereaderwiki.com/en/Bell_XV-15

APPENDIX

YouTube Links for ANSYS Analyses and Different Scenarios

- **CFD analysis**
  https://youtu.be/aLZoxzyfIME

- **Structural analysis**
  https://youtu.be/-NVRXoUiR2A

- **Takeoff and Cargo Loading**
  https://youtu.be/kK1EyTvJ31E

- **Cargo Unloading Scenario**
  https://youtu.be/x-Hs8K6vfPo

- **Landing Scenario**
  https://youtu.be/NDMb4wmn5yU

Helicopter Group Weights & Sizing Codes

```
clc;
clear all;
format long

Wcrew=180;          % Weight of the crew in Ib (80 kg+ 8 kg luggage)
Wpayload= 551;      % Weight of the payload in Ib (80 kg + 15 kg luggage)
Wfuel=2703;         % Weight of the fuel in Ib
L=7;                % Length of the fuselage in ft
W= 5.5;             % Width of the fuselage in ft
H=7.8;              % Height of the fuselage in ft
DL= 14.0;           % Values of the disk loadings in lb/ square ft ( also 3 lb / sq.ft)
Vtip=700;           % Blade tip speed (from design specification 0f 194 m/s) in ft/s
Vc=215;             % Cruise velosity in knots
HP=1000;            % Engine's Hp
sol=0.1;            % solidity of the main rotor
K=4.65;
V=365;              %forward velocity in ft/s
Wdry=2*355.38;      %two engines, one engine dry weight 161.2 kg
Wwing=700;          %317.2 kg
Wstabilizer=517.7;
```

```
Wg=7165;       % initial guess of gross take off weight in Ib

%%Loop
x=1;
 while x==1
%%Rotor group (?R)
R=sqrt((Wg)/(pi*DL)); % Radius for the Main Rotor in ft
Wr= 1.7*((Wg)^(0.342))*(R^(1.58))*(sol^(0.63));


%%Power plant section group (?PS)
omega=Vtip/R;                % Rotational speed in
Wps=0.00155*((Wg)^(1.07))*(omega^(0.54));

%%Mechanical drive system group (?DS)
Wds=42.4*(((2*HP*R)/(Vtip))^(0.763));

%%Flight control group (?FC)
Wfc=0.0226*((Wg)^(0.712))*(Vc^(0.653));
%%Avionics (average value)
Wavi=150;
%%Furnishing & equipment
Weq=13*((Wg/1000)^1.3);

%%Landing gear group (?LG)
Wlg=0.0475*((Wg)^(0.975));

%%Fuselage group (?F)
Wf=0.21*(Wg)^0.598*R^0.942;


%%Empty weight using the weight group method

Wempty=Wr+Wps+Wds+Wfc+Wlg+Wf+Wavi+Wdry+Wwing+Wstabilizer+Weq;

%%Gross take off weight
```

```
WgTOW= Wempty+ Wcrew+Wpayload+Wfuel


%%Absolute error
Abs_error= abs(WgTOW-Wg)/WgTOW*100;          %Absolute relative error
 if Abs_error <=0.0001
     x=2;
   else
      Wg=(WgTOW+Wg)/2;
   end

 end

 %%Momentum Theory for Thrust, Power and Torque in Hover conditions
 T= WgTOW;                % Thrust is equal to the weight in Hover in Ib
 A= pi*R*R;               % Area of the disk
 Rho=0.0765;              % Density at sea level in lb/ft^3
 Vi= sqrt(T/(2*Rho*A));     % Induced Velocity
 k=1.15;
 Cdo=0.016;
 f=16.48;
 Phover=(k*Vi*T)+1/8*(sol*Cdo);                % Induced Power in foot-pounds/second
 P_tot=(k*Vi*T)+(1/8*(sol*Cdo))*(1+K*((V/Vtip).^2))+0.5*Rho*(V.^3)*f;
 Q=P_tot/omega;                          % Torque (in lbft)
 Pprofile=(1/8*(sol*Cdo))*(1+K*((V/Vtip).^2));    %profile power
 Pind=(k*Vi*T);                          %induced power
 kg_value=0.45*WgTOW                     %lb to kg conversion
```

Power Estimation in Forward Flight(Blade Element Theory in FF: Torque and Power)

```
clc
clear all

CD_0 = 0.0116;
rho = 15.5*10^-4; %slug/ft^3
k = 1.15;
K = 4.6;
```

```
T = 7535.8 ; %lbf
f = 16.48 ; %ft^2, flat plate drag area
sigma = 0.1 ; %soldity
R = 13 ; % main rotor radius in ft
A = pi*R^2; %ft^2
V_tip=700; %ft/s
omega = V_tip/R ; %rotational speed 1/rad

dV = 1;
v=[];
Q1=[];
Q2=[];
Q3=[];
Q4=[];
for V = 0 : dV : 500*0.911 %forward velocity
v = [v,V];
   v_i = sqrt((-0.5*V^2+0.5*sqrt(V^4+4*((T/(2*rho*A))^2))));  %ft/s induced velocity component

   P_i = (k*v_i*T)*0.0018 ;                          %induced power
   P_profile = (0.125*sigma*CD_0*rho*A*(omega*R)^3*(1+K*(V/(omega*R))^2))*0.0018;%profile power
   P_parasite = (0.5*rho*V^3*f)*0.0018;                    %parasite power

   P = P_i + P_profile + P_parasite                     %Power required hp

   Q1=[Q1,P];
   Q2=[Q2,P_i];
   Q3=[Q3,P_profile];
   Q4=[Q4,P_parasite];
end
plot(v,Q1,'b-','linewidth',1); hold on;
plot(v,Q2,'m-','linewidth',1);hold on;
plot(v,Q3,'c-','linewidth',1); hold on;
plot(v,Q4,'k-','linewidth',1);hold on;
plot(xlim, 2000*[1 1],'-r','linewidth',1.1);
legend('Required Power','Induced Power','Profile Power','Parasite Power','Available Power')
xlabel('Forward Flight Velocity, V[ft/s]');
ylabel('Power Required, P[hp]');
```

Airfoil Selection Codes

VR-7 Airfoil Analysis

```
clc
clear all
clf
nu = 1.789*10^-5; %N s/m^2
R = 3.96;
R_min = 0.05*R;
ro = 1.225; %kg/m^3
A = pi*R^2; %m^2
W = 3857; %kg
T = W*9.81; %N
V_tip = 215; %m/s
Numblade = 3;
omega = 343.74; %rad/s
c = 0.2524; %m
P = 1000*745.7; %W
dr = 0.001;
theta_tw = 0; %rad
V_i = sqrt(T/(ro*A*2)); %m/s induced velocity component
U_p = V_i; %out of plane velocity component
sigma = (Numblade*c)/(pi*R); %solidity
k = 1.15; %correction factor for power
```

```
theta0 = 4.24; %degree
theta_tw = 0; %degree
C_T1 = 0; %C_T EULER
C_T2 = 0; %C_T EULER
C_T3 = 0; %C_T EULER
C_T4 = 0; %C_T EULER
C_Pi1 = 0;
C_Pi2 = 0;
C_Pi3 = 0;
C_Pi4 = 0;
Re_max = ro*V_tip*c/nu;
Re_min = ro*omega*R_min*c/nu;
C_T = T/(ro*A*V_tip^2); %mom theory
```

```
%the matrix values to plot the graphs
v=[];
Q1=[];
Q2=[];
Q3=[];
Q4=[];
Q5=[];
for r = 0.05:dr:0.076
v=[v,r];
U_t1 = omega*r*R;
phi1 = U_p/U_t1;
lambda1 = phi1*r;
C_l_alfa1 = 0.1203; %
C_d01 = 0.0169; %
dC_T1 = 0.5*sigma*C_l_alfa1*r^2*dr;
e = lambda1*dC_T1; %dC_P incremental
C_Pi1 = C_Pi1 + e;
theta1 = theta0+r*theta_tw; %rad
a = 0.5*sigma*C_l_alfa1*(theta1*r^2-lambda1*r)*dr;
C_T1 = C_T1+a;
alpha_effective1 = (theta1 - phi1);
Q1=[Q1,theta1];
Q2=[Q2,round(lambda1*10000)/10000;];
Q3=[Q3,alpha_effective1];
Q4=[Q4,dC_T1];
Q5=[Q5,e];
end
for r = 0.077:dr:0.188
v=[v,r];
U_t2 = omega*r*R;
phi2 = U_p/U_t2;
lambda2 = phi2*r;
C_l_alfa2 =0.0990 ; %
C_d02 = 0.0102; %
dC_T2 = 0.5*sigma*C_l_alfa2*r^2*dr;
f = lambda2*dC_T2; %dC_P incremental
C_Pi2 = C_Pi2 + f;
theta2 = theta0+r*theta_tw; %degree
```

```
b = 0.5*sigma*C_l_alfa2*(theta2*r^2-lambda2*r)*dr;
C_T2 = C_T2+b;
alpha_effective2 = (theta2 - phi2);
Q1=[Q1,theta2];
Q2=[Q2,round(lambda2*10000)/10000;];
Q3=[Q3,alpha_effective2];
Q4=[Q4,dC_T2];
Q5=[Q5,f];
end
for r = 0.189:dr:0.237
v=[v,r];
U_t3 = omega*r*R;
phi3 = U_p/U_t3;
lambda3 = phi3*r;
C_l_alfa3 =0.1097 ; %
C_d03 = 0.0062; %
dC_T3 = 0.5*sigma*C_l_alfa3*r^2*dr;
g = lambda3*dC_T3; %dC_P incremental
C_Pi3 = C_Pi3 + g;
theta3 = theta0+r*theta_tw; %degree
c = 0.5*sigma*C_l_alfa3*(theta3*r^2-lambda3*r)*dr;
C_T3 = C_T3+c;
alpha_effective3 = (theta3 - phi3);
Q1=[Q1, theta3];
Q2=[Q2,round(lambda3*10000)/10000;];
Q3=[Q3,alpha_effective3];
Q4=[Q4,dC_T3];
Q5=[Q5, g];
end
for r = 0.238:dr:1
v=[v,r];
U_t4 = omega*r*R;
phi4 = U_p/U_t4;
lambda4 = phi4*r;
C_l_alfa4 =0.1127 ; %
C_d04 = 0.0054; %
dC_T4 = 0.5*sigma*C_l_alfa4*r^2*dr;
h = lambda4*dC_T4; %dC_P incremental
```

```
C_Pi4 = C_Pi4 + h;
theta4 = theta0+r*theta_tw; %degree
d = 0.5*sigma*C_l_alfa4*(theta4*r^2-lambda4*r)*dr;
C_T4 = C_T4+d;
alpha_effective4 = (theta4 - phi4);
Q1=[Q1,theta4];
Q2=[Q2,round(lambda4*10000)/10000];
Q3=[Q3,alpha_effective4];
Q4=[Q4,dC_T4];
Q5=[Q5,h];
end
C_T_tot = C_T1+C_T2+C_T3+C_T4; %EULER
C_Pi_tot = C_Pi1+C_Pi2+C_Pi3+C_Pi4;
dC_T_tot = dC_T1+dC_T2+dC_T3+dC_T4;
C_d0_mean = (C_d01+C_d02+C_d03+C_d04)/4;
C_p0 = 0.125*sigma*C_d0_mean;
T_final = C_T_tot*(omega*R)^2*ro*A; %Newton
P_i = (omega*R)^3*ro*A*C_Pi_tot; %Watt
P_0 = C_p0*ro*A*V_tip^3; %Watt
P_tot = k*P_i + P_0;
FM = P_i/P_tot;
%plots
figure (1);
plot(v,Q1);
title('Local Pitch Angle vs. Local Radius')% make title
xlabel('Local Radius') % x-axis label
ylabel('Local Pitch Angle, degree')% y-axis label
figure (2);
plot(v,Q2);
title('Local Inflow Angle vs. Local Radius')% make title
xlabel('Local Radius') % x-axis label
ylabel('Local Inflow Angle, degree')% y-axis label
axis([0 1 0 .05])
figure (3);
plot(v,Q3);
title('Local Effective Angles of Attack vs. Local Radius')% make title
xlabel('Local Radius') % x-axis label
ylabel('Local Effective Angles of Attack, degree')% y-axis label
```

```
figure (4);
plot(v,Q4);
title('Incremental Thrust Coefficient vs. Local Radius')% make title
xlabel('Local Radius') % x-axis label
ylabel('Incremental Thrust Coefficient')% y-axis label
figure (5);
plot(v,Q5);
title('Incremental Induced Power Coefficient vs. Local Radius')% make title
xlabel('Local Radius') % x-axis label
ylabel('Incremental Induced Power Coefficient')% y-axis label
```

NACA0012 Airfoil Analysis

```
clc
clear all
clf
nu = 1.789*10^-5; %N s/m^2
R = 3.96;
R_min = 0.05*R;
ro = 1.225; %kg/m^3
A = pi*R^2; %m^2
W = 3857; %kg
T = W*9.810; %N
V_tip = 215; %m/s
Numblade = 3;
omega = 343.74; %rad/s
c = 0.2524; %m
P = 1000*745.7; %W
dr = 0.001;
theta_tw = 0; %rad
V_i = sqrt(T/(ro*A*2)); %m/s induced velocity component
U_p = V_i; %out of plane velocity component
sigma = (Numblade*c)/(pi*R); %solidity
k = 1.15; %correction factor for power
```

```
theta0 =5.22; %degree
theta_tw = 0; %degree
C_T1 = 0; %C_T EULER
C_T2 = 0; %C_T EULER
```

```
C_T3 = 0; %C_T EULER
C_T4 = 0; %C_T EULER
C_Pi1 = 0;
C_Pi2 = 0;
C_Pi3 = 0;
C_Pi4 = 0;
Re_max = ro*V_tip*c/nu;
Re_min = ro*omega*R_min*c/nu;
C_T = T/(ro*A*V_tip^2); %mom theory
%the matrix values to plot the graphs
v=[];
Q1=[];
Q2=[];
Q3=[];
Q4=[];
Q5=[];
for r = 0.05:dr:0.076
v=[v,r];
U_t1 = omega*r*R;
phi1 = U_p/U_t1;
lambda1 = phi1*r;
C_l_alfa1 = 0.0685; %
C_d01 = 0.0169; %
dC_T1 = 0.5*sigma*C_l_alfa1*r^2*dr;
e = lambda1*dC_T1; %dC_P incremental
C_Pi1 = C_Pi1 + e;
theta1 = theta0+r*theta_tw; %rad
a = 0.5*sigma*C_l_alfa1*(theta1*r^2-lambda1*r)*dr;
C_T1 = C_T1+a;
alpha_effective1 = (theta1 - phi1);
Q1=[Q1,theta1];
Q2=[Q2,round(lambda1*10000)/10000;];
Q3=[Q3,alpha_effective1];
Q4=[Q4,dC_T1];
Q5=[Q5,e];
end
for r = 0.077:dr:0.188
v=[v,r];
```

```
U_t2 = omega*r*R;
phi2 = U_p/U_t2;
lambda2 = phi2*r;
C_l_alfa2 =0.1128 ; %
C_d02 = 0.0102; %
dC_T2 = 0.5*sigma*C_l_alfa2*r^2*dr;
f = lambda2*dC_T2; %dC_P incremental
C_Pi2 = C_Pi2 + f;
theta2 = theta0+r*theta_tw; %degree
b = 0.5*sigma*C_l_alfa2*(theta2*r^2-lambda2*r)*dr;
C_T2 = C_T2+b;
alpha_effective2 = (theta2 - phi2);
Q1=[Q1,theta2];
Q2=[Q2,round(lambda2*10000)/10000;];
Q3=[Q3,alpha_effective2];
Q4=[Q4,dC_T2];
Q5=[Q5,f];
end
for r = 0.189:dr:0.237
v=[v,r];
U_t3 = omega*r*R;
phi3 = U_p/U_t3;
lambda3 = phi3*r;
C_l_alfa3 =0.0821 ; %
C_d03 = 0.0062; %
dC_T3 = 0.5*sigma*C_l_alfa3*r^2*dr;
g = lambda3*dC_T3; %dC_P incremental
C_Pi3 = C_Pi3 + g;
theta3 = theta0+r*theta_tw; %degree
c = 0.5*sigma*C_l_alfa3*(theta3*r^2-lambda3*r)*dr;
C_T3 = C_T3+c;
alpha_effective3 = (theta3 - phi3);
Q1=[Q1, theta3];
Q2=[Q2,round(lambda3*10000)/10000;];
Q3=[Q3,alpha_effective3];
Q4=[Q4,dC_T3];
Q5=[Q5, g];
end
```

```
for r = 0.238:dr:1
v=[v,r];
U_t4 = omega*r*R;
phi4 = U_p/U_t4;
lambda4 = phi4*r;
C_l_alfa4 =0.0877 ; %
C_d04 = 0.0054; %
dC_T4 = 0.5*sigma*C_l_alfa4*r^2*dr;
h = lambda4*dC_T4; %dC_P incremental
C_Pi4 = C_Pi4 + h;
theta4 = theta0+r*theta_tw; %degree
d = 0.5*sigma*C_l_alfa4*(theta4*r^2-lambda4*r)*dr;
C_T4 = C_T4+d;
alpha_effective4 = (theta4 - phi4);
Q1=[Q1,theta4];
Q2=[Q2,round(lambda4*10000)/10000];
Q3=[Q3,alpha_effective4];
Q4=[Q4,dC_T4];
Q5=[Q5,h];
end
C_T_tot = C_T1+C_T2+C_T3+C_T4; %EULER
C_Pi_tot = C_Pi1+C_Pi2+C_Pi3+C_Pi4;
dC_T_tot = dC_T1+dC_T2+dC_T3+dC_T4;
C_d0_mean = (C_d01+C_d02+C_d03+C_d04)/4;
C_p0 = 0.125*sigma*C_d0_mean;
T_final = C_T_tot*(omega*R)^2*ro*A; %Newton
P_i = (omega*R)^3*ro*A*C_Pi_tot; %Watt
P_0 = C_p0*ro*A*V_tip^3; %Watt
P_tot = k*P_i + P_0;
FM = P_i/P_tot;
%plots
figure (1);
plot(v,Q1);
title('Local Pitch Angle vs. Local Radius')% make title
xlabel('Local Radius') % x-axis label
ylabel('Local Pitch Angle, degree')% y-axis label
figure (2);
plot(v,Q2);
```

```
title('Local Inflow Angle vs. Local Radius')% make title
xlabel('Local Radius') % x-axis label
ylabel('Local Inflow Angle, degree')% y-axis label
axis([0 1 0 .05])
figure (3);
plot(v,Q3);
title('Local Effective Angles of Attack vs. Local Radius')% make title
xlabel('Local Radius') % x-axis label
ylabel('Local Effective Angles of Attack, degree')% y-axis label
figure (4);
plot(v,Q4);
title('Incremental Thrust Coefficient vs. Local Radius')% make title
xlabel('Local Radius') % x-axis label
ylabel('Incremental Thrust Coefficient')% y-axis label
figure (5);
plot(v,Q5);
title('Incremental Induced Power Coefficient vs. Local Radius')% make title
xlabel('Local Radius') % x-axis label
ylabel('Incremental Induced Power Coefficient')% y-axis label
```

2D drawings of Helly-800 design with the dimensions

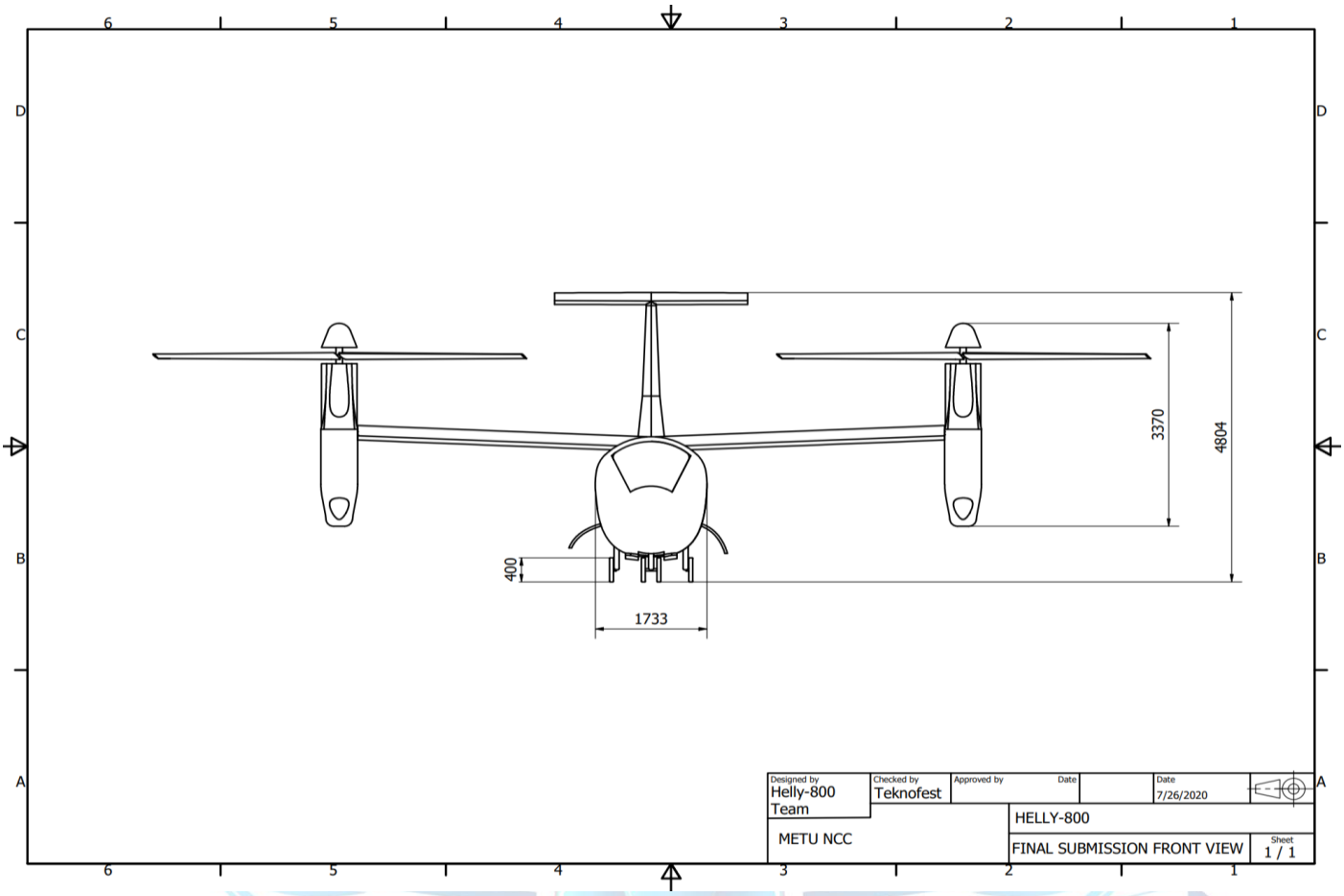

Figure : Front view

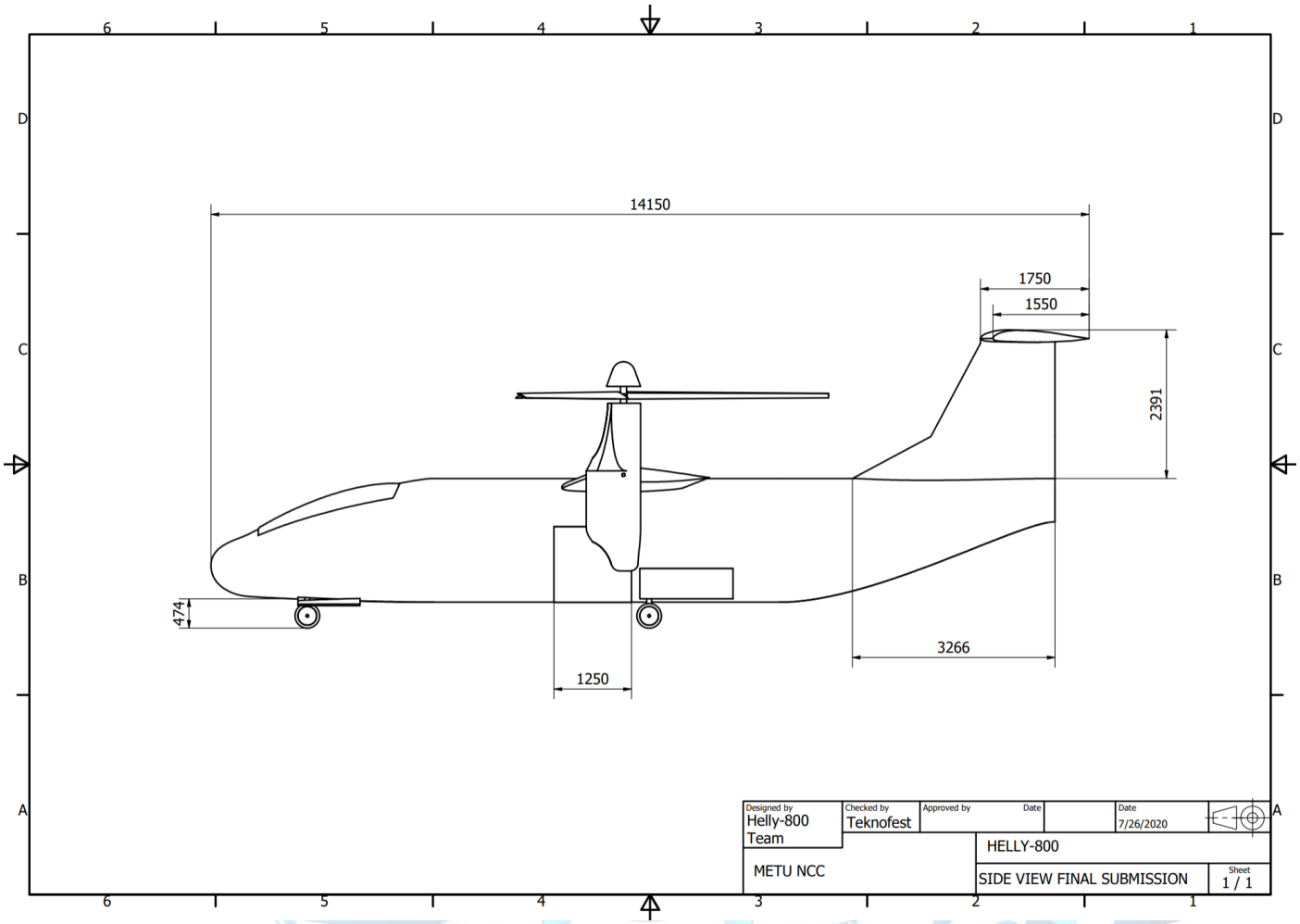

Figure : Side view

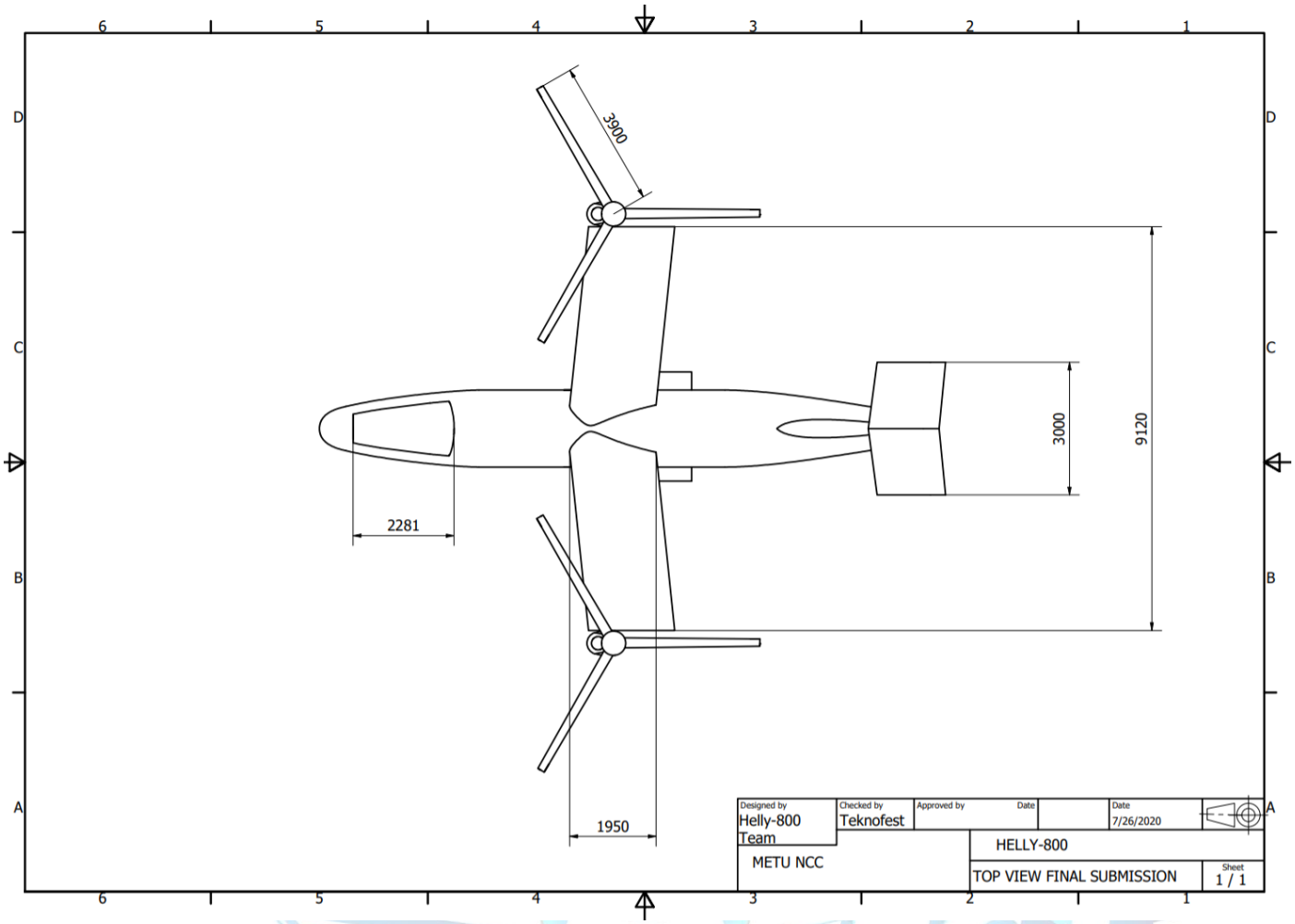

Figure : Top view